Article:
Grey, William George orcid.org/0000-0001-8209-5645, Rio-Machin, Ana, Casado, Pedro et al. (11 more authors) (2022) CKS1 inhibition depletes leukemic stem cells and protects healthy hematopoietic stem cells in acute myeloid leukemia. Science Translational Medicine. eabn3248. ISSN 1946-6242

https://doi.org/10.1126/scitranslmed.abn3248

Title: CKS1 inhibition depletes leukemic stem cells and protects healthy hematopoietic stem cells in acute myeloid leukemia

Authors: William Grey[1,2]*, Ana Rio-Machin[3], Pedro Casado[4], Eva Grönroos[5], Sara Ali[1], Juho J. Miettinen[6], Findlay Bewicke-Copley[3], Alun Parsons[6], Caroline A. Heckman[6], Charles Swanton[5,7], Pedro R. Cutillas[4], John Gribben[8], Jude Fitzgibbon[3], Dominique Bonnet.[1]*

Affiliations:

1. Haematopoietic Stem Cell Laboratory, The Francis Crick Institute, London, NW1 1AT, U.K.
2. York Biomedical Research Institute, Department of Biology, University of York, York, YO10 5DD, U.K.
3. Centre for Genomics and Computational Biology, Bart's Cancer Institute, Queen Mary University of London, London, EC1M 6BQ, U.K.
4. Cell signalling and proteomics group, Centre for Genomics and Computational Biology, Barts Cancer Institute, Queen Mary University of London, London, EC1M 6BQ, U.K.
5. Cancer evolution and genome instability laboratory, The Francis Crick Institute, London, NW1 1AT, U.K.
6. Institute for Molecular Medicine Finland – FIMM, HiLIFE – Helsinki Institute of Life Science, iCAN Digital Precision Cancer Medicine Flagship, University of Helsinki, Helsinki, Finland.
7. UCL Cancer Institute, 72 Huntley St, London WC1E 6DD.
8. Centre for Haemato-Oncology, Bart's Cancer Institute, Queen Mary University of London, London, EC1M 6BQ, U.K.

* Corresponding authors: dominique.bonnet@crick.ac.uk, william.grey@york.ac.uk

Single Sentence Summary: Targeting CKS1 has opposing effects in normal and malignant hematopoiesis, protecting normal HSCs while reducing the leukemic stem cell pool.

Abstract

Acute myeloid leukemia (AML) is an aggressive hematological disorder comprising a hierarchy of quiescent leukemic stem cells (LSCs) and proliferating blasts with limited self-renewal ability. AML has a dismal prognosis, with extremely low two-year survival rates in the poorest cytogenetic risk patients, primarily due to the failure of intensive chemotherapy protocols to deplete LSCs, and toxicity of therapy towards healthy hematopoietic cells. We studied the role of CKS1-dependent protein degradation in primary human AML and healthy hematopoiesis xenograft models in vivo. Using a small molecule inhibitor (CKS1i), we demonstrate a dual role for CKS1-dependent protein degradation in reducing AML blasts in vivo, and importantly depleting LSCs, whilst inhibition of CKS1 has the opposite effect on normal hematopoiesis, protecting normal hematopoietic stem cells from chemotherapeutic toxicity. Proteomic analysis of responses to CKS1i demonstrate that inhibition of CKS1 in AML leads to hyperactivation of RAC1 and accumulation of lethal reactive oxygen species, whereas healthy hematopoietic cells enter quiescence in response to CKS1i, protecting hematopoietic stem cells. Together these findings demonstrate CKS1-dependent proteostasis is a key vulnerability in malignant stem cell biology.

Main Text

Introduction

Acute myeloid leukemia (AML) is a heterogeneous, aggressive disease of the hematopoietic system, arising from hematopoietic stem/progenitor cells. The average two-year survival rate is 5-15% in poor risk, older patients with AML patients (>65yr), demonstrating an unmet critical need for new therapeutic approaches*(1)*. Fundamentally, leukemic stem cells (LSCs), the cancer stem cells (CSCs) of the hematopoietic system, are the origins of relapse in AML*(2)* and show substantial plasticity from *de novo* disease through to relapse*(3)*. Therefore, new approaches targeting AML LSCs are critical for improving AML prognosis. Recent developments, such as targeting the anti-apoptotic protein BCL2 using Venetoclax, have demonstrated that therapies affecting protein networks hold great promise for a wide variety of cancers, including poor risk classification patients with AML*(4, 5)*. Yet resistance still emerges through LSC adaptations*(6, 7)*.

The key aim of CSC-targeted therapy is to selectively reduce CSCs without negatively affecting normal stem cells. Improved understanding of the biological differences between normal and malignant stem cells is needed to achieve selective CSC targeting, without toxicity to normal stem cells.

We previously reported a regulatory axis between the cyclin-dependent kinase (CDK) subunits Cks1 and Cks2, and the mixed lineage leukemia 1 protein (Mll1). Mll1 is a key protein hijacked during neoplastic transformation of the hematopoietic system*(8)* and important for regulation of normal and cancer stem cells from multiple different tissues*(9, 10)*. Cks1 and Cks2 have multifaceted overlapping and independent roles in balancing protein homeostasis, so called "proteostasis", throughout the cell cycle, ensuring correct G0/G1 transition*(11)*, chromatin separation*(12–14)* and DNA repair*(11, 15, 16)*. Cks1 and Cks2 also possess CDK-independent functions, in concert with the Skp1/2, cullin, F-box containing complex (SCF^{SKP2}) and anaphase promoting complex (APC^{CDC20}) E3 ubiquitin ligases, important for selective protein degradation*(11, 12, 17)*.

The ubiquitin proteosome system (UPS) is a highly regulated system that controls protein degradation and is essential for correct cellular protein homeostasis. It has been reported that up to 80% of cellular proteins are degraded by the UPS, demonstrating its importance in proliferation, survival, differentiation and drug resistance *(18–21)*. Targeting the UPS has proved elusive in hematopoietic disorders. Broad spectrum inhibitors of protein degradation, such as Bortezomib, have shown increased toxicity without improvement of overall survival *(22)*. Targeting less broad cullin-dependent protein degradation, using drugs such as Pevonedistat, was initially promising *(23, 24)*, but trials have failed to significantly improve overall survival*(25*). We previously demonstrated in vitro that pan-cullin inhibition can lead to cell cycle arrest in AML, whereas more specific inhibition of protein degradation targeting CKS1 leads to cell death *(8)*. Indeed, small molecule inhibitors targeting SCF-SKP2-CKS1 are able to stabilise p27 protein and block cancer cells in G2/M phase of the cell cycle, leading to cell death, rather than cell cycle arrest *(8, 26, 27)*.

In the current study, we investigated the sensitivity of poor risk AML – a sub-classification with few treatment options – to protein phosphorylation and degradation inhibitors to reveal CKS1-dependent vulnerabilities. We demonstrate efficacy in reducing the LSC pool through the inhibition of CKS1-dependent protein degradation either as a single treatment or in combination with standard chemotherapy. In contrast,

103 CKS1 inhibition had the opposite effect on normal hematopoiesis, improving stem cell
104 functionality and conferring protection from chemotherapeutic toxicity. Together, these
105 findings offer a new treatment for eradicating drug resistant LSCs whilst preserving
106 healthy hematopoiesis.
107
108 *Results*
109
110 **High expression of *CKS1B* dictates sensitivity of bulk AML to inhibition of CKS1-**
111 **dependent protein degradation**
112 The overexpression of *CKS1B* correlates with poor prognosis in a variety of solid
113 tumors*(28–30)*, but is an indeterminant factor in AML (Fig. S1A-D) despite a broad
114 range of expression in normal and malignant hematopoiesis across multiple cohorts
115 and datasets (Fig. S1E). *CKS1B* expression varied significantly between both normal
116 and malignant hematopoiesis and within different hematopoietic subtypes (Kruksal-
117 Wallis, $P<2.2^{-16}$, Supp. Table S1), with intermediate expression in healthy
118 hematopoietic stem cells (HSCs), and a broad range of expression in most AML
119 cytogenetic subtypes compared to one of its key upstream proteostatic regulation
120 partners *SKP2* (Fig. S1F).
121 We hypothesized that high *CKS1B* expression in AML may provide a selective
122 susceptibility to inhibition of either CDK-CKS1-dependent phosphorylation or SCF-
123 CKS1-dependent protein degradation by an $SCF^{SKP2\text{-}CKS1}$ E3 ligase inhibitor, hereafter
124 referred to as CKS1i*(26, 27)*. To address this key question, we screened a cohort of
125 cytogenetically poor risk AMLs, spanning a variety of morphological (French-
126 American-British, FAB) and molecular subtypes, with a broad range of *CKS1B*
127 expression (Figure 1A, Supp. Table S2). AMLs were tested for sensitivity to a range
128 of CDK inhibitors, a broad-spectrum protein degradation inhibitor (Bortezomib), and
129 specific inhibitors of the $SCF^{SKP2\text{-}CKS1}$ E3 ubiquitin ligase complex (Pevonedistat and
130 CKS1i; Figure 1A-B, Fig. S2A-B, Supp. Table S3).
131 Whilst CDK inhibition resulted in fewer than 50% of primary AML samples
132 demonstrating robust drug sensitivity (DSS), whereas protein degradation inhibitors
133 demonstrated increased drug sensitivity of AML blasts grown in vitro (Fig. S2A). Since
134 failure of broad-spectrum protein degradation inhibitors has been reported previously,
135 and we reported induction of quiescence rather than cell death by Pevonedistat*(8)*, we
136 investigated whether inhibition of more specific CKS1-dependent protein degradation

137 could be more effective. Indeed, knockdown of *CKS1B* in AML results in dose- and
138 time-dependent reduction in viability (Fig. S2C-E), and CKS1i drug sensitivity directly
139 correlated with *CKS1B* expression in poor risk patients with AML patients (R=0.61,
140 p=0.0078; Figure 1C), with clear separation of high and low DSS (Fig S2F). Separating
141 patients at the 50th percentile by *CKS1B* expression revealed significantly increased
142 drug sensitivity in *CKS1B*^{high} versus *CKS1B*^{low} patients with AML patients (P=0.0035,
143 Fig S2F), indicating that RNA expression of *CKS1B* could be a selection criterion for
144 targeting SCF$^{SKP2\text{-}CKS1}$ dependent protein degradation in AML. Additional
145 characterization of patient phenotypes indicated that white blood counts at diagnosis
146 are similar between patients with *CKS1B*^{high} and *CKS1B*^{low} expressing tumors and
147 CKS1i responders and non-responders, and both groupings covered an array of
148 mutational profiles, with a multivariate analysis demonstrating only *CKS1B* expression
149 correlates with in vitro CKS1i sensitivity (Fig. S2G-I, Supp. Tables S4 , S5 & S6).
150 In order to investigate the effect of CKS1i on primary patient AML in vivo, we selected
151 five primary patient samples with a range of *CKS1B* expression to engraft in
152 immunodeficient NSG mice (Supp. Table S2). A single course of CKS1i (10mg/kg, 5
153 days treatment I.P.) significantly reduced the leukemic burden in mice engrafted with
154 patient AMLs carrying the highest *CKS1B* expression (AML12 P=0.001 and AML21
155 P=0.04). A trend towards reduced AML burden was seen at intermediate level of
156 *CKS1B* expression (AML26), but CKS1 inhibition had no significant effect on bulk AML
157 in mice for patient samples with the lowest *CKS1B* expression (AML27 and AML32;
158 Figure 1D). As such, *CKS1B* expression directly correlated with acute tumor reduction
159 in vivo (R=-0.446; Figure 1E). All CKS1i treated AML xenografts showed a delay in
160 AML bone marrow colonisation over time, regardless of tumor reduction immediately
161 post-CKS1i treatment (Fig. S3) and improved overall survival compared to untreated
162 controls (Figure 1F-J). This indicates that CKS1i treatment had additional effects
163 beyond acutely reducing bulk leukemic burden of *CKS1B*^{high} AML in mice.
164
165 **CKS1-dependent degradation is a specific vulnerability in leukemic stem cells**
166 Whilst reducing leukemic blast count is the current backbone of clinical
167 chemotherapeutic protocols and required to release leukemic cell-mediated
168 suppression of normal hematopoietic cells, these approaches do not target quiescent
169 LSCs, the subset of cells at the origin of relapse in vivo*(31)*. The observed effect on
170 bone marrow colonisation and overall survival upon CKS1i treatment in *CKS1B*^{low} AML

171 xenograft mice could indicate a specific mechanism of action of CKS1i on LSCs.
172 Indeed, LSCs are rare and bulk *CKS1B* expression does not account for LSC-specific
173 *CKS1B* dependency.
174 Transcriptomic analysis of patient AMLs at single cell resolution revealed subsets of
175 AML expressing *CKS1B* clustering with LSC genes (Fig. S4A-B). To better quantify
176 LSC-dependency on CKS1 in primary patient AML, we investigated CKS1 protein
177 abundance at single cell resolution. Mass cytometry-based *t*-stochastic neighbor
178 embedding demonstrated strong association of CKS1 protein abundance with a range
179 of immunophenotypic and functional LSC markers (Figure 2A, Fig. S4C). When
180 focussing on primary patient immunophenotypic LSC subpopulations
181 ($CD200^+CD99^+CLL\text{-}1^+CD123^+CD117^+$, Fig. S5A), CKS1 protein abundance was
182 significantly higher than bulk AML (P=0.0002, Figure 2B). Similarly,
183 immunophenotypic LSCs had increased abundance of proteins important for both
184 stem cell functionality and drug resistance, such as BCL2, active β-catenin (Fig. S5B).
185 To assess the functional effect of CKS1i on LSCs we used the leukemic-long-term
186 culture initiating cell assay (L-LTC-IC). All patient samples showed significant
187 reduction in L-LTC-IC frequency, demonstrating a direct effect of CKS1i treatment on
188 LSC functionality (P<0.0001, Figure 2C-D, Fig. S5C). In addition, primary human AML
189 cells recovered from AML26 xenografts were secondarily transplanted in limiting
190 dilution. No xenografts carrying previously CKS1i treated AMLs showed overt signs of
191 ill-health, whereas control xenografts died within 150 days (Figure 2E). Analysis of
192 human bone marrow engraftment of secondary xenograft mice demonstrated
193 reduction in LSC frequency by CKS1i treatment (Figure 2F, Fig. S5D). In agreement,
194 when cultured in vitro, patient AML samples treated with CKS1i show increased
195 apoptosis in the LSC compartment (Figure 2G) and a reduction in LSCs compared to
196 total AML blasts (Figure 2H).
197 These data demonstrate that LSCs have high concentrations of CKS1 and CKS1i is
198 efficient at targeting the LSC compartment. The reduction of LSCs by CKS1i indicates
199 a clear route to combating AML in all patients independent of bulk *CKS1B* expression.
200
201 **CKS1 inhibition protects healthy hematopoiesis from chemotherapeutic toxicity**
202 Contrary to primary patient AML LSCs and AML cell lines, healthy umbilical cord blood
203 derived $CD34^+$ and the more primitive $CD34^+CD45RA^-$ compartment did not undergo

204 apoptosis in response to CKS1i (Figure 3A). Where AML cells accumulated in S-G2-
205 M phases of the cell cycle (Fig. S5E), healthy CD34$^+$ cells increased p27 abundance
206 in primitive fractions (Figure 3B) and became significantly more quiescent (P=0.01,
207 Figure 3C), leading to fewer cells in culture over time (Figure 3D).
208 By inducing quiescence and limiting cell growth, CKS1i would reduce the ability to
209 incorporate nucleotide analogues, such as Cytarabine, and the toxicity of
210 topoisomerase inhibitors, such as Doxorubicin. We hypothesized that this could place
211 CKS1i as a "chemoprotective agent" during classical induction chemotherapy in AML,
212 protecting healthy hematopoietic cells from chemotherapeutic killing.
213 To investigate this hypothesis, we engrafted healthy umbilical cord blood derived
214 CD34$^+$ cells in NSG mice and treated the mice with the clinical chemotherapy protocol
215 of cytarabine plus doxorubicin (5+3 days)*(33)*, in the presence or absence of CKS1i
216 (Figure 3E). Human bone marrow engraftment increased in untreated control mice
217 between weeks 4 and 6 as expected. Treatment at week 4 with doxorubicin/cytarabine
218 (DA) reduced bone marrow engraftment by week 6, reducing the expansion of human
219 cells compared to control, but addition of CKS1i (DAC) was able to rescue this effect,
220 returning expansion of human cells similar to controls (Figure 3F-G). Better
221 engraftment at week 6 was complemented by a reduction in apoptotic human cells in
222 the bone marrow of recipient mice (Figure 3H-I), indicating that CKS1i treatment
223 prevents DA-induced cell death in normal hematopoietic cells. Secondary
224 transplantation of human cells obtained from primary treatment mice showed an
225 increase in HSC frequency after CKS1i treatment, rescuing DA effects on HSCs
226 (Figure 3J). This indicates that CKS1i protects healthy HSCs from chemotherapy
227 induced depletion.
228 Outside of the hematopoietic system a key side-effect of induction chemotherapy for
229 AML is severe gut by-toxicity, often resulting in intestinal dysfunction and infection*(34,*
230 *35)*. In agreement with the effects on normal HSPCs, DA treatment induced increased
231 proliferation of intestinal crypts (Fig. S6A-B) and resulted in fewer LGR5$^+$ crypts post-
232 chemotherapy (Fig. S6C-D). Both phenotypes were rescued by the addition of CKS1i,
233 returning proliferation and number of LGR5$^+$ crypts to control numbers.
234 These data demonstrate that CKS1i has the opposite effect on healthy tissue
235 compared to AML, and suppression of growth induced by CKS1i can be
236 chemoprotective for healthy tissue during clinically used chemotherapy.
237

238 **Divergent cellular responses to CKS1i by healthy and malignant hematopoietic**
239 **cells**
240 To investigate the mechanism by which CKS1i induces divergent responses between
241 healthy and malignant hematopoietic cells, we carried out proteomic analysis of
242 *CKS1B*^{high} AML cell lines, which demonstrate direct correlation between *CKS1B*
243 expression and CKS1i response, phenocopying primary patient AML (Fig. S7, Supp.
244 Table S6), and umbilical cord blood derived healthy CD34^{+} HSPCs, with and without
245 CKS1i treatment in vitro (1μM; Figure 4A).
246 CKS1i treatment induced ~7.5x more differentially abundant proteins in THP-1 cells
247 compared to healthy CD34^{+} (Figure 4B-C). Differentially abundant cell cycle proteins
248 demonstrated the divergent responses to CKS1i by healthy and malignant
249 hematopoietic cells. Indeed, downregulation of cell cycle drivers and protein
250 translation machinery in CD34^{+} cells and upregulation of S phase promoting proteins
251 in AML cells, with relatively few overlapping proteins (<10%), explains divergent cell
252 cycle responses (Figure 4D-E).
253 Furthermore, key proteins differentially abundant in CD34^{+} cells and not AML were
254 integrated in three pathways fundamental to normal hematopoiesis: Wnt signalling,
255 cell cycle control and NFκB signalling (Figure 4D, Fig. S8A). To investigate the
256 changes in these key signalling pathways at single cell resolution we carried out mass
257 cytometry with a panel of cell surface and intracellular markers covering signalling
258 pathways important for HSPC proliferation, differentiation and stem cell self-renewal
259 *(36)*.
260 Pseudo-bulk-level multidimensional scaling demonstrated a convergence of individual
261 CD34^{+} donors upon treatment with CKS1i (Fig. S8B). These differences in CD34^{+} cells
262 after CKS1i treatment were largely due to a reduction in abundance of intracellular
263 signalling markers (Fig. S8C), particularly IκBα/NFκB signalling, CREB and mTOR
264 phosphorylation (Figure 4F, Fig. S8D) and reduced proliferating cells (Figure 3C).
265 Changes that were not observed in bulk AML or AML LSCs in response to CKS1i (Fig.
266 S8E). In addition, the protein abundance of differentiation regulators such as PU.1
267 were also reduced (Fig. S8D), indicating a potential block in differentiation. Fewer cells
268 had active non-phosphorylated β-catenin, demonstrating that the Wnt pathway – a
269 fundamental pathway requiring a tight balance for normal hematopoiesis to proceed –
270 was suppressed (Figure 4G, Fig. S8D).

271 Reduction of metabolically active markers like mTOR^{pS2448}, inflammatory responses
272 including NFkB^{pS529}, and suppression of the translation machinery in our mass
273 spectrometry analyses resulted in reduction of protein translation in CKS1i treated
274 CD34^{+} cells (Figure 4H). Together, these signalling pathways are fundamental to the
275 control of stress responses and particularly important to prevent the accumulation of
276 lethal ROS in HSCs*(37)*. In agreement, CKS1i treatment reduced intracellular ROS in
277 CD34^{+} cells (Figure 4I). CKS1i-dependent reduction of ROS surpassed that of NAC
278 treatment, with no additive effects of CKS1i and NAC (Figure 4I). This led to improved
279 stem cell frequency of CD34^{+} cells cultured in the presence of CKS1i (Fig. S8F).
280 The substantial changes in these key pathways are hallmarks of suppression of growth
281 and differentiation, rather than an induction of cell death by CKS1i, confirming our
282 functional data that HSC frequency increases when treated with CKS1i alone and
283 CKS1i protects HSCs from the toxicity of Cytarabine/Doxorubicin (Figure 3I, Fig. S8F).
284

285 **CKS1i induces an integrated molecular switch in AML cells driving RAC1**
286 **activity and NADP/H metabolism**

287 Proteomic alterations mediated by CKS1i in AML revealed key changes beyond S
288 phase accumulation, with modulators of the Ras-related C3 botulinum toxin substrate
289 1 (RAC1) and nicotinamide adenine dinucleotide phosphate (NADP/H) activity
290 differentially abundant between control and CKS1i treated cells (Figure 5A, Fig. S9A-
291 B).
292 Total RAC1 protein abundance was increased (Fig. S9C), as well as key interactors,
293 such as Paxillin and CRK, after CKS1i treatment (Figure 5A). Mechanistically,
294 inhibition of the SCF$^{SKP2\text{-}CKS1}$ complex led to accumulation of p27 (Fig. S9D), which
295 inhibits RHOA activity (Figure 5B, Fig. S9E) *(38)*. This reduced the activity of RAC1-
296 GTPase activating proteins (RAC-GAPs), to maintain RAC1 in its GTP bound state
297 *(39)*, working in concert with RAC1 signalling pathway members to increase the
298 amount of RAC1-GTP in AML after CKS1i treatment (Figure 5C, Fig. S9F).
299 RAC1-GTP together with NOXA(p67^{Phox}) regulates NADP to NADPH conversion –
300 providing a pool for NADPH oxidases to produce ROS*(40)*. CKS1i altered a range of
301 NADP/H metabolic regulators (Figure 5A). Thus, we evaluated the abundance and
302 ratio of NADP/NADPH upon CKS1i treatment. CKS1i induced a dose dependent
303 increase of NADPH in AML cells (Figure 5D-E, Fig. S10A-D). The accumulation of
304 NADPH is dependent on RAC1-GTP activity, as CKS1i induction of NADPH was

305 rescued by the RAC1 inhibitor NSC23766 (NSC, Figure 5D-E. Fig. S10A-D).
306 Sensitivity of the RHOA-RAC1 axis to CKS1i correlated with p27 stabilization (Fig.
307 S9D) and IC_{50} values in *CKS1B*^{high} and *CKS1B*^{low} AML cell lines (Fig. S7),
308 further demonstrating the dose-dependent sensitivity to CKS1i based on *CKS1B*
309 expression. Together, these data demonstrate that inhibition of the $SCF^{SKP2\text{-}CKS1}$
310 complex induces an integrated molecular switch, with regulation of RAC1/NADPH
311 activity maintained by convergent signalling pathways.
312
313 **Inhibition of SCF-SKP2-CKS1 drives lethal ROS accumulation in AML**
314 CKS1i-induced RAC1 activity and NADPH accumulation led to increased intracellular
315 ROS in AML cell lines (Figure 5F-G, Fig. S10E-F), a phenotype conserved upon
316 *CKS1B* knockdown (Figure 5H-J), indicating that CKS1 is critical to balance ROS
317 abundance. Inhibition of RAC1 in cell lines rescued intracellular ROS accumulation
318 induced by CKS1i or *CKS1B* knockdown (Figure 5F-J, Fig. S10E-F), and at higher
319 doses was able to rescue CKS1i induced reduction in cell viability (Figure 5K-L, Fig.
320 S10G-H).
321 Primary AML cells grown in vitro demonstrated similar sensitivity to CKS1i treatment,
322 with induction of apoptosis in both bulk AML (Figure 5M) and importantly the LSC
323 fraction of samples (Figure 5N). However, whereas RAC1 inhibition could improve the
324 growth of AML, CKS1i effects on LSCs were dominant, maintaining LSC depletion
325 during double treatment (Figure 5N, Fig S10I-K).
326 As the antioxidant N-acetyl-L-cysteine (NAC) is well known to scavenge intracellular
327 ROS to reverse the negative effects of ROS on HSCs/LSCs, we tested whether NAC
328 could reduce intracellular ROS accumulation and rescue survival. Indeed, NAC was
329 able to reduce intracellular ROS in CKS1i treated AML cell lines (Figure 6A-C), and at
330 higher doses NAC reversed CKS1i-dependent reduction in viability, demonstrating
331 that CKS1i kills AML through accumulation of lethal ROS (Figure 6D-E). Additionally,
332 increased intracellular ROS by CKS1i, or knockdown of *CKS1B,* led to induction of
333 *CDKN1A* expression (Figure 6F-I), a known downstream effect of ROS causing cell
334 cycle arrest and apoptosis.
335 Patient LSCs must maintain low ROS for survival*(41)*, and treatment of primary patient
336 AML in vitro with CKS1i induced apoptosis in the LSC fraction and reduced both the
337 proportion and total number of LSCs compared to control conditions (Figure 6J-L, Fig.

338 S10L-M). NAC treatment rescued CKS1i-induced LSC depletion in three out of four
339 cases, returning LSC number similar to control conditions (Figure 6J-L).
340 These data demonstrate that AML requires $SCF^{SKP2\text{-}CKS1}$ functions to maintain a
341 balance of intracellular ROS, which is critical for LSC maintenance in vivo. Ultimately,
342 the increase in ROS, and the reduction in LSCs driven by CKS1i, indicates a clear
343 pathway to target *CKS1B*^{high} LSCs in vivo, regardless of bulk *CKS1B* status in AML.
344
345 **Combining CKS1 inhibition with induction chemotherapy simultaneously**
346 **reduces LSCs, protects normal HSCs and improves overall survival**
347 To test the potential for combining classical DA chemotherapy with CKS1i (DAC) in
348 AML, we transplanted NSG mice with primary AML samples of varying *CKS1B*
349 expression (Figure 7A). After stratifying for engraftment at week 4, we treated the mice
350 with either DA or DAC. One-week post chemotherapy, xenografts showed strong
351 reduction in leukemic burden in both DA and DAC treatment cohorts for all AMLs,
352 regardless of *CKS1B* expression (Figure 7B). At the same time point, resident murine
353 $CD45^{+}$ cells co-extracted from aspirated tibias had higher colony forming potential
354 upon the addition of CKS1i compared to untreated mice and DA treated mice (Figure
355 7C), indicating that CKS1i treatment could selectively reduce AML, whilst
356 simultaneously protecting normal HSPCs colony forming potential. Overall, DA
357 treatment was only able to improve survival of one patient AML xenograft, due to the
358 extensive by-toxicity of the treatment combined with AML burden in NSG mice.
359 Addition of CKS1i improved overall survival of all patient AML xenografts, with many
360 xenograft mice surviving up to 150 days (Figure 7D, Fig. S11A-D).
361 Examination of the normal hematopoietic compartment of xenografted mice at the end
362 point of survival revealed a reduction in total number of long-term HSCs (LT-HSCs) in
363 the DA treated group, whereas addition of CKS1i to DA abolished this effect, rescuing
364 LT-HSC number (Figure 7E). In addition, the serial colony forming ability of normal
365 murine HSPCs was improved in DAC conditions, indicating that rescued HSPCs were
366 functional (Figure 7F).
367 We and others have documented the refractory nature of LSCs to induction
368 chemotherapy*(42)*, and we set out to investigate the potential conflict or beneficial
369 contribution between DA and CKS1i. In ex vivo conditions, both *CKS1B*$^{high\ \&\ low}$ AMLs
370 (Figure 7G) showed a reduction in total cell number one week after DA or DAC
371 treatment (Figure 7H), yet whilst DA treatment enriched for L-LTC-IC frequency in

372 three of the six patient samples, addition of CKS1i reduced L-LTC-IC frequency in all
373 patients (Figure 7I & Fig S11E-F).
374 Finally, to investigate the reduction in LSC frequency conferred by CKS1i in vivo, we
375 engrafted AML cells obtained from AML26 and AML32, which had the smallest
376 improvement in overall survival after chemotherapy, in secondary recipient mice at
377 limiting dilutions. Whilst control AMLs retained strong LSC frequency and showed
378 robust engraftment after six weeks, frequency was increased by DA treatment in
379 AML26 and was reduced in AML32 (Figure 7J-K, Fig. S12A-B). The addition of CKS1i
380 counteracted the effect of DA by decreasing the LSC frequency in AML26 and further
381 reducing LSC frequency in AML32 compared to DA and control mice, demonstrating
382 strong reduction in LSCs after CKS1i treatment independent of the response to DA
383 treatment (Figure 7J-K, Fig. S12A-B).
384 Overall secondary DA-AML mice survived longer than controls, and DAC-AML treated
385 mice showed further improvement in survival, with no overt signs of sickness at 150
386 days in six of seven cases for both AML26 and AML32 (Figure 7L, Fig. S12C).
387 Together, these data indicate that inhibition of CKS1-dependent protein degradation
388 in combination with frontline chemotherapy is a more effective strategy to reduce the
389 LSC pool, whilst protecting normal HSCs from chemotherapeutic toxicity.
390
391 *Discussion*
392
393 The difficulty of selectively targeting CSCs whilst simultaneously preserving normal
394 stem cells is a major challenge in cancer therapy, and the study of normal and
395 malignant hematopoietic stem cells has played a major role in understanding CSC
396 biology*(43)*. In this study, we demonstrate that CKS1 is a key protein in this paradigm,
397 with LSCs expressing higher CKS1 than most AML blasts, providing a selective
398 vulnerability of LSCs to inhibition of the $SCF^{SKP2\text{-}CKS1}$ E3 ubiquitin ligase complex, while
399 sparing normal HSCs from chemotherapeutic toxicity.
400 Poor risk AML is a heterogeneous group of cytogenetic abnormalities with very limited
401 treatment options and extremely low overall survival rates*(1)*, even accounting for
402 newer therapies, such as Venetoclax plus Azacitidine *(4, 5)*. While gene expression
403 profiles, particularly those with single cell resolution, are improving our understanding
404 of AML heterogeneity, the origins of relapse and revealing new clinical targets*(31)*, the
405 role of proteostasis has been comparatively understudied*(44, 45)*. The selective

406 reduction of leukemic cells by CKS1 inhibition demonstrates that precisely targeting
407 proteostatic regulators can be a new avenue in AML therapy.
408 Here we demonstrate that CKS1 regulates LSC viability through RAC1/NADPH/ROS
409 pathways, fundamental in amplifying extrinsic and intrinsic signals in normal
410 hematopoiesis and AML*(6, 46)*, and critical to metastatic disease across cancer*(47)*.
411 The balance of intracellular ROS in normal and malignant hematopoietic stem cells
412 has been of great interest in recent years*(37, 41)*, and changes in mitochondrial
413 functions due to *RAS* mutations and nicotinamide-NAD metabolism underline the
414 critical role for this pathway in primary patient resistance to Venetoclax*(6, 7)*. The
415 induction of ROS in AML upon CKS1 inhibition demonstrates that the balance of
416 CKS1-dependent protein degradation is key to maintaining stress responses in AML.
417 This, together with LSCs requiring low ROS to maintain their stem cell potential,
418 explains the strong reduction in LSC frequency conferred by CKS1i in primary patient
419 AML (Figures 2 and 7).
420 The effect of CKS1i on normal hematopoiesis is clearly different to the effects
421 observed in AML (Figure 3). Indeed, cell cycle blockage is highly beneficial, as patients
422 treated with induction chemotherapy, which targets cycling cells, suffer from severe
423 toxicity and cytopenia upon treatment. Classical induction chemotherapy is known to
424 reduce the pool of hematopoietic progenitors, whilst quiescent HSCs are refractory to
425 treatment, but ultimately undergo senescence*(48)*. It has previously been reported that
426 deletion of *p27* in murine progenitors increased cycling and potency *(49)*. In
427 agreement, we found that increased p27 protein and the accompanying cell cycle
428 arrest of HSPCs by CKS1i could prevent DA reduction of normal cells in vivo (Figure
429 3), and in the context of AML could rescue the reduction in HSCs induced by
430 chemotherapy (Figure 7). Importantly, CKS1i treatment also induced changes in
431 fundamental HSPC signalling pathways involved in stem cell potency and response to
432 stress. The overall suppression of key growth and activation cellular markers led to an
433 opposite phenotype to that seen in AML cells, with a reduction in intracellular ROS
434 and an increase in normal HSC frequency (Figure 4). In addition, CKS1i also rescues
435 negative effects of induction chemotherapy on intestinal crypts (Fig. S6), a major issue
436 associated with patient chemotherapeutic by-toxicity*(34, 35)*. Considering that older
437 poor risk patients with AML patients (>65 years), who comprise the majority of AML
438 cases, are ineligible for intensive chemotherapy *(50, 51)*, the reduction in toxicity

439 towards healthy tissue conferred by CKS1i during DA treatment has the potential to
440 improve outcomes independent of direct AML effects.
441 The non-AML-intrinsic mechanism of action and effects on normal HSPCs by CKS1i
442 may also implicate further components in the bone marrow niche. We and others have
443 detailed the evolving bone marrow niche in hematological malignancies*(52)*, and the
444 diverse repertoire of proteostatic machinery affected by CKS1i has the potential to
445 affect cell competition in the leukemic bone marrow microenvironment by affecting
446 normal HSPCs as well as stromal components.
447 Thus, the inhibition of CKS1-dependent protein degradation holds excellent promise
448 for AML therapy, both as a single agent towards *CKS1B*^{high} AML, and in combination
449 with induction chemotherapy in remaining AML cases. Reports of *CKS1B*
450 overexpression correlating with outcome in other solid cancer types*(28, 30)*, and ways
451 to modulate CKS1 activity*(53)*, indicate that proteostatic targeting, through this axis,
452 holds much hope for future cancer therapy.
453
454 *Limitations of study*
455 The main limitation of our study is that we focus on a cohort of poor risk patients with
456 AML which, despite covering a variety of cytogenetic and FAB subtypes, does not
457 cover the full heterogeneity of patients with AML seen in the clinic. Further work will
458 be needed to evaluate the efficacy of CKS1i on intermediate and good risk AML patient
459 groups. As the combination of doxorubicin and cytarabine is quite toxic to the
460 immunodeficient mice, it is not possible to combine this treatment with a
461 preconditioning of the mice by sublethal irradiation. We were thus limited to testing
462 combination approaches with patient AML samples capable of engrafting
463 immunodeficient mice without prior conditioning. To mitigate this limitation, we tested
464 a range of patient AML samples in ex vivo and in vitro conditions, to confirm all
465 phenotypes through multiple assays.
466
467 *Methods*
468
469 **Study design**
470 This study aimed to investigate the sensitivity of poor risk AML to inhibition of CKS1-
471 dependent protein degradation, as well as the potential side effect of this inhibitor on
472 normal hematopoietic stem and progenitor cells. 32 primary poor risk AML patient

473 samples were obtained from St Bartholomew's Hospital as part of the poor risk AML
474 consortium, of which 21 were suitable for drug screening and five were able to robustly
475 engraft immunodeficient mouse models. We have performed several experiments
476 using different approaches to address these objectives. We first analyzed whether the
477 effect of CKS1i correlates to gene expression of *CKS1* in bulk AML samples. We also
478 evaluated the protein expression of CKS1 in leukemic stem cells using mass cytometry
479 analysis. We then evaluated the effect of CKS1i on primary poor risk AML and on
480 normal hematopoietic stem/progenitor cells in vivo using immunodeficient mice. We
481 also performed proteomic analysis on both normal and leukemic cells to investigate
482 the mechanisms of action of CKS1i and used a RAC1 inhibitor (NSC23766) or N-
483 Acetyl L Cysteine (NAC) to rescue the effects of CKS1i. Detailed below are all criteria
484 for experimental cut-offs (e.g. mouse endpoint censure), number of cells used,
485 blinding (all experiments were blinded during data collection unless otherwise stated)
486 and statistical tests used.
487
488 **Primary AML and UCB samples**
489 AML samples were obtained after informed consent at St Bartholomew's Hospital
490 (London, U.K.) at the time of diagnosis as part of the Bart's Cancer Institute Poor-Risk
491 AML consortium. Full details of patient information are provided in Supplementary
492 Table 1. Live mononuclear cells (MNCs) were isolated by density centrifugation using
493 Ficoll-Paque (GE healthcare). Prior to culture or xenotransplantation, AML cells were
494 depleted for T-cells using the Easysep T-cell depletion kit (StemCell Technologies).
495 Umbilical Cord Blood (UCB) was obtained from full-term deliveries after informed
496 consent, at the Royal London Hospital (London, U.K.). MNCs were isolated by density
497 centrifugation using Ficoll-Paque (GE healthcare). Cells were selected for $CD34^+$
498 using the Easysep $CD34^+$ enrichment kit (StemCell Technologies). Purity was
499 confirmed by flow cytometry. The collection and use of all human samples were
500 approved by the East London Research Ethical Committee (REC:06/Q0604/110) and
501 in accordance with the Declaration of Helsinki.
502
503 **Patient derived xenografts (PDX) and in vivo drug treatment**
504 All animal experiments were performed under the project license (PPL 70/8904)
505 approved by the Home Office of the UK and in accordance with the Francis Crick
506 institute animal ethics committee and ARRIVE guidelines. NOD-SCID IL2Rynull

507 (NSG) mice were originally a gift from Dr L. Schultz (Jackson Laboratory). These mice
508 were rederived and bred since then at The Francis Crick Institute Biological Resources
509 Facility.
510 Primary AML samples ($1x10^6$ – $5x10^6$ cells total) or UCB-$CD34^+$ ($5x10^4$ cells total)
511 were injected intravenously (I.V.) into unconditioned 10-12 weeks old female or male
512 NSG mice. After 4 weeks, engraftment was assessed by bone marrow aspiration from
513 long bones whilst mice were under isoflurane anaesthesia. Mice were stratified
514 according to engraftment and sex and assigned to treatment and control groups
515 accordingly. Mice were treated as indicated with 10mg/kg CKS1i (Skp2-Cks1 E3
516 ligase inhibitor, Merck Millipore) intraperitoneal injection (I.P.) for 5 days, DA
517 (doxorubicin/cytarabine, 1.5mg/kg/10mg/kg respectively, Sigma Aldrich), doxorubicin
518 on days 1-3, cytarabine on days 1-5 co-injected I.V.*(33)*. Mice were scored for
519 engraftment over the experimental course by bone marrow aspiration and for overall
520 survival according to U.K. home office license protocols and following CRUK guidance
521 (>20% peak body weight loss, overt signs of sickness/mortality).
522
523 **Leukemic/Normal Long-term culture initiating cell (L-LTC-IC) assay**
524 These experiments were performed as originally published by our group*(54)*. For all
525 co-culture experiments, MS-5 stromal cells were seeded two days prior to AML/UCB
526 cell addition at $4x10^5$ cells/ml to reach confluence at the time of irradiation. One day
527 prior to AML/UCB addition, MS-5 stromal cells were irradiated with 7Gy and culture
528 media was exchanged. On the day of starting co-culture, AML cells were plated at
529 $2x10^5$ cells/ml in meylocult H5100 (StemCell Technologies) supplemented with IL-3,
530 G-CSF and TPO (all 20ng/ml; Peprotech). UCB cells were plated at $2x10^5$ cells/ml in
531 myelocult H5100 (StemCell Technologies). Half media changes were performed once
532 per week without disrupting the feeder layer. At the start of week two, indicated drug
533 treatments were added at 2x concentration in the half media change once. For L-LTC-
534 CAFC assays, all cells were harvested at day 14 and sorted for live $hCD45^+mSca\text{-}1^-$
535 cells. Resulting cells were seeded in co-culture with fresh MS-5 stromal cells in a 96
536 well plate in a limiting dilution range (200,000 to 1,000) in 10 replicates and cultured
537 for a further 5 weeks. At the end of the co-culture period cobblestone area forming
538 cells were scored and L-LTC-IC frequency was calculated using the ELDA (Extreme
539 Limiting Dilution Analysis) function in the Statmod R package.

540 For LTC-IC assays, media was continuous changed each week until week five, when
541 cultures were harvested and live hCD45$^+$mSca-1$^-$ cells were sorted. Resulting cells
542 were seeded in co-culture with fresh MS-5 stromal cells in a 96 well plate in a limiting
543 dilution range (10,000 to 100) in 10 replicates and cultured for a further three weeks.
544 At week eight, myelocult H5100 was replaced with Methocult methycellulose
545 (StemCell Technologies H4434) for a further two weeks, after which wells were scored
546 for colony-forming units and LTC-IC frequency was calculated using the ELDA
547 (Extreme Limiting Dilution Analysis) function in the Statmod R package.
548
549 **Protein translation assays**
550 Protein translation was measured using the OP-Puromycin protein translation kit (Life
551 Technologies). AML cell lines were seeded at $2x10^5$ cells/ml one day prior to treatment
552 with the indicated drugs (day 0). The following day (day 1), drugs were added to culture
553 wells at the indicated concentration. The next day (day 2), 10 μM OP-Puromycin was
554 added to culture wells for one hour under culture conditions (37C, 5% CO_2). Cells were
555 washed three times in ice-cold PBS and fixed in 4% paraformaldehyde (Sigma Aldrich)
556 at room temperature for 15 mins in the dark. Cells were washed three times in PBS
557 and permeabilised in PBS + 0.5% Triton X-100 (Sigma Aldrich) for 15 mins. Cells were
558 washed twice in Click-IT reaction buffer wash solution and stained as per the
559 manufacturer's instructions (Life Technologies). Abundance of OP-Puromycin was
560 assessed using flow cytometry on a BD Fortessa FACS analyser.
561
562 **Intracellular ROS staining**
563 Intracellular reactive oxygen species were assayed using the CellRox deep red
564 reagent (Life Technologies). AML cell lines were seeded at $2x10^5$ cells/ml one day
565 prior to treatment with the indicated drugs (day 0). The following day (day 1), drugs
566 were added to culture wells. The next day (day 2), CellRox deep red was added to
567 each well at a final concentration of 5uM and verapamil was added at a final
568 concentration of 50 μM. Cells were continued to be incubated in the same conditions
569 (37C, 5% CO_2) for 1hr. After incubation, cells were collected from wells and washed
570 three times in PBS + 1%FBS + 50 μM verapamil and finally resuspended in PBS + 1%
571 FBS + 50 μM verapamil + DAPI (0.1μg/ml) before analysis on a BD Fortessa FACS
572 analyser.
573

574 **NADP/NADPH assays**

575 Total NADP/H and NADPH were measured using the NADP/NADPH colorimetric
576 assay kit (Abcam). AML cell lines were seeded at $2x10^5$ cells/ml one day prior to
577 treatment with the indicated drugs (day 0). The following day (day 1), drugs were
578 added to culture wells at the indicated concentration and cells were harvested after 8
579 hours. All cells were collected from the wells and washed three times in ice-cold PBS.
580 Cells were lysed in NADP/NADPH extraction buffer by performing two freeze/thaw
581 cycles (20 mins on dry ice followed by 10 mins at room temperature). Lysates were
582 centrifuged at 13,000g for 10minutes and the supernatant was retained. Lysate
583 supernatant was split in half, with one half remaining on ice and the other half
584 incubated at 60C for 30mins to remove $NADP^+$. Total NADP/H (NADPt) and NADPH
585 only lysates were run in 96 well plates with freshly made standards as per the
586 manufacturers' instructions. NADP/NADPH ratio was calculated as (NADPt-
587 NADPH)/NADPH.

588

589 **Mass Cytometry**

590 CyTOF preparation and analysis was carried out as per our previous publication *(36)*.
591 Cultured cells were washed in ice-cold PBS three times and incubated with 5μM
592 Cisplatin (Fluidigm) to mark dead cells. Cells were washed three times in ice-cold PBS
593 and fixed in 1.6% formaldehyde (Sigma Aldrich). Fixed cells were surface stained with
594 the relevant antibodies (resources table) for two hours at room temperature followed
595 by three washes with PBS. Cells were permeabilised in 1ml Perm buffer III (BD
596 biosciences) on ice for 30mins, washed three times in ice-cold PBS and incubated
597 with the relevant intracellular antibodies (resources table) overnight at 4ºC with gentle
598 rotation. Resulting cells were wash three times in ice-cold PBS and stained with
599 100nM Iridium in PBS + 0.1% Saponin (Riedel-de Haen) overnight before analysis on
600 a Helios Mass Cytometer (Fluidigm). All control and CKS1i treated samples were
601 prepared simultaneously with equal buffers, antibodies and fixation.

602

603 **Publicly available datasets**

604 *CKS1B* expression in normal and malignant hematopoiesis was obtained through
605 Bloodspot.eu. Overall survival and stratification for *CKS1B* expression was calculated
606 from data obtained from The Cancer Genome Atlas (TCGA). AML cell line RNA

607 sequencing data was obtained from the EBI Expression Atlas (RNA-seq of 934 Human
608 cancer cell lines from the Cancer Cell Line Encyclopedia).
609
610 **Statistics and data interpretation**
611 Results shown are +/-SEM unless otherwise indicated. To compare treatment versus
612 control in all in vitro and in vivo experiments, a Student's *t*-test was used as indicated
613 in the figure legend with N number indicated. For all comparisons, unpaired *t*-tests
614 were undertaken unless otherwise indicated. All repeat samples presented are from
615 biological replicates of distinct samples/xenotransplantations. Survival analyses were
616 carried out using the "survminer" package on R to calculate significance between
617 Kaplan-Meier curves and Hazard ratios. Kaplan Meier graphs were plotted using
618 Graphpad Prism. Correlation analyses were carried out using the "performance
619 analytics" and "corrplot" packages in R. Multiple DSS comparisons with *CKS1B*
620 expression were carried out with pairwise complete observations using Spearman,
621 Pearson and Kendall correlation coefficients. Individual correlations for *CKS1B* vs
622 DSS or IC_{50} were plotted using Graphpad Prism. Stem cell frequency was calculated
623 using the extreme limiting dilution analysis (ELDA) function in the "statmod" R
624 package*(55)*. Pathway analysis and enrichment was run through MetaCore
625 (genego.com) and network interactions produced on String (string-db.org). CyTOF
626 analysis was conducted using the CATALYST package on gated live, single cells.
627
628
629 *Acknowledgements*
630 We would like to acknowledge the Francis Crick core flow cytometry, cell services and
631 biological research facility STPs. We would like to acknowledge Drs R. Hynds, H
632 Wood, D. Taussig & Prof. P. Parker for their critical feedback on the manuscript.
633 Graphical abstract was created with BioRender.com.
634
635 *Funding*
636 This works was supported partly by Cancer Research UK (FC001115 to DB), the UK
637 Medical Research Council (FC001115 to DB), the Wellcome Trust (FC001115 to DB),
638 a CRUK program grant (C15966/A24375 to JF & DB) and Leukaemia U.K.
639 (2021/JGF/002 to WG). For the purpose of Open Access, the authors have applied a

Author contributions

W.G. Conceived the study, designed and carried out experiments, analyzed data and wrote the manuscript. A.R-M. Analyzed patient data. P.C-I. Carried out mass spectrometry analyses. E.G. carried out experiments and analyzed data. J.J.M. Designed and carried out experiments. S.A. Analyzed data. F.B-C. Analyzed data. A.P. Designed and carried out experiments. C.A.H. Undertook drug screening. P.C. Undertook mass spectrometry analyses. C.S. Provided LGR5 mice and gut preparations. J.G. Provided patient samples and data. J.F. Provided patient samples and data. D.B. Conceived the study and wrote the manuscript. All authors provided critical feedback on the manuscript pre-submission.

Competing interests

C.S. acknowledges grant support from AstraZeneca, Boehringer-Ingelheim, Bristol Myers Squibb, Pfizer, Roche-Ventana, Invitae (previously Archer Dx Inc - collaboration in minimal residual disease sequencing technologies), and Ono Pharmaceutical. He is an AstraZeneca Advisory Board member and Chief Investigator for the AZ MeRmaiD 1 and 2 clinical trials and is also chief investigator of the NHS Galleri trial. He has consulted for Achilles Therapeutics, Amgen, AstraZeneca, Pfizer, Novartis, GlaxoSmithKline, MSD, Bristol Myers Squibb, Illumina, Genentech, Roche-Ventana, GRAIL, Medicxi, Metabomed, Bicycle Therapeutics, Roche Innovation Centre Shanghai, and the Sarah Cannon Research Institute. C.S. had stock options in Apogen Biotechnologies and GRAIL until June 2021, and currently has stock options in Epic Bioscience, Bicycle Therapeutics, and has stock options and is co-founder of Achilles Therapeutics. P.C. is co-founder and director of Kinomica Ltd.

Patents: C.S. holds patents relating to assay technology to detect tumour recurrence (PCT/GB2017/053289); to targeting neoantigens (PCT/EP2016/059401), identifying patient response to immune checkpoint blockade (PCT/EP2016/071471), determining HLA LOH (PCT/GB2018/052004), predicting survival rates of patients with cancer (PCT/GB2020/050221), identifying patients who respond to cancer treatment (PCT/GB2018/051912), US patent relating to detecting tumour mutations (PCT/US2017/28013), methods for lung cancer detection (US20190106751A1) and

both a European and US patent related to identifying insertion/deletion mutation targets (PCT/GB2018/051892).

Data and materials availability

All data associated with this study are present in the paper or supplementary materials. The mass spectrometry proteomics data have been deposited to the ProteomeXchange Consortium via the PRIDE partner repository (PXD022754 and 10.6019/PXD022754).

Supplementary Materials

Supplementary materials and methods

Supplementary
Fig. S1. To S12.

Supplementary table S1. To S7.

References

1. H. Döhner, D. J. Weisdorf, C. D. Bloomfield, D. L. Longo, Ed. Acute Myeloid Leukemia, *N. Engl. J. Med.* **373**, 1136–1152 (2015).

2. L. I. Shlush, A. Mitchell, L. Heisler, S. Abelson, S. W. K. Ng, A. Trotman-Grant, J. J. F. Medeiros, A. Rao-Bhatia, I. Jaciw-Zurakowsky, R. Marke, J. L. McLeod, M. Doedens, G. Bader, V. Voisin, C. Xu, J. D. McPherson, T. J. Hudson, J. C. Y. Wang, M. D. Minden, J. E. Dick, Tracing the origins of relapse in acute myeloid leukaemia to stem cells, *Nature* (2017), doi:10.1038/nature22993.

3. T. C. Ho, M. LaMere, B. M. Stevens, J. M. Ashton, J. R. Myers, K. M. O'Dwyer, J. L. Liesveld, J. H. Mendler, M. Guzman, J. D. Morrissette, J. Zhao, E. S. Wang, M. Wetzler, C. T. Jordan, M. W. Becker, Evolution of acute myelogenous leukemia stem cell properties after treatment and progression, *Blood* (2016), doi:10.1182/blood-2016-02-695312.

4. C. D. DiNardo, I. S. Tiong, A. Quaglieri, S. MacRaild, S. Loghavi, F. C. Brown, R. Thijssen, G. Pomilio, A. Ivey, J. M. Salmon, C. Glytsou, S. A. Fleming, Q. Zhang, H.

709 Ma, K. P. Patel, S. M. Kornblau, Z. Xu, C. C. Chua, X. Chen, P. Blombery, C.
710 Flensburg, N. Cummings, I. Aifantis, H. Kantarjian, D. C. S. Huang, A. W. Roberts, I.
711 J. Majewski, M. Konopleva, A. H. Wei, Molecular patterns of response and treatment
712 failure after frontline venetoclax combinations in older patients with AML, *Blood* **135**,
713 791–803 (2020).
714 5. C. D. DiNardo, B. A. Jonas, V. Pullarkat, M. J. Thirman, J. S. Garcia, A. H. Wei, M.
715 Konopleva, H. Döhner, A. Letai, P. Fenaux, E. Koller, V. Havelange, B. Leber, J.
716 Esteve, J. Wang, V. Pejsa, R. Hájek, K. Porkka, Á. Illés, D. Lavie, R. M. Lemoli, K.
717 Yamamoto, S.-S. Yoon, J.-H. Jang, S.-P. Yeh, M. Turgut, W.-J. Hong, Y. Zhou, J.
718 Potluri, K. W. Pratz, Azacitidine and Venetoclax in Previously Untreated Acute
719 Myeloid Leukemia, *N. Engl. J. Med.* **383**, 617–629 (2020).
720 6. C. L. Jones, B. M. Stevens, D. A. Pollyea, R. Culp-Hill, J. A. Reisz, T. Nemkov, S.
721 Gehrke, F. Gamboni, A. Krug, A. Winters, S. Pei, A. Gustafson, H. Ye, A. Inguva, M.
722 Amaya, M. Minhajuddin, D. Abbott, M. W. Becker, J. DeGregori, C. A. Smith, A.
723 D'Alessandro, C. T. Jordan, Nicotinamide Metabolism Mediates Resistance to
724 Venetoclax in Relapsed Acute Myeloid Leukemia Stem Cells, *Cell Stem Cell* (2020),
725 doi:10.1016/j.stem.2020.07.021.
726 7. B. M. Stevens, C. L. Jones, D. A. Pollyea, R. Culp-Hill, A. D'Alessandro, A.
727 Winters, A. Krug, D. Abbott, M. Goosman, S. Pei, H. Ye, A. E. Gillen, M. W. Becker,
728 M. R. Savona, C. Smith, C. T. Jordan, Fatty acid metabolism underlies venetoclax
729 resistance in acute myeloid leukemia stem cells, *Nat. Cancer* , 1–12 (2020).
730 8. W. Grey, A. Ivey, T. A. Milne, T. Haferlach, D. Grimwade, F. Uhlmann, E. Voisset,
731 V. Yu, The Cks1/Cks2 axis fine-tunes Mll1 expression and is crucial for MLL-
732 rearranged leukaemia cell viability, *Biochim. Biophys. Acta - Mol. Cell Res.* **1865**,
733 105–116 (2018).
734 9. R. C. Rao, Y. Dou, Hijacked in cancer: The KMT2 (MLL) family of
735 methyltransferases*Nat. Rev. Cancer* **15**, 334–346 (2015).
736 10. J. Grinat, J. Heuberger, R. O. Vidal, N. Goveas, F. Kosel, A. Berenguer-Llergo,
737 A. Kranz, A. Wulf-Goldenberg, D. Behrens, B. Melcher, S. Sauer, M. Vieth, E. Batlle,
738 A. F. Stewart, W. Birchmeier, The epigenetic regulator Mll1 is required for Wnt-driven
739 intestinal tumorigenesis and cancer stemness, *Nat. Commun.* (2020),
740 doi:10.1038/s41467-020-20222-z.
741 11. M. Frontini, A. Kukalev, E. Leo, Y.-M. M. Ng, M. Cervantes, C.-W. W. Cheng, R.
742 Holic, D. Dormann, E. Tse, Y. Pommier, V. P. C. C. Yu, The CDK Subunit CKS2

743 Counteracts CKS1 to Control Cyclin A/CDK2 Activity in Maintaining Replicative
744 Fidelity and Neurodevelopment, *Dev. Cell* **23**, 356–370 (2012).
745 12. R. Wolthuis, L. Clay-Farrace, W. van Zon, M. Yekezare, L. Koop, J. Ogink, R.
746 Medema, J. Pines, Cdc20 and Cks direct the spindle checkpoint-independent
747 destruction of cyclin A, *Mol Cell* **30**, 290–302 (2008).
748 13. H. S. Martinsson-Ahlzen, V. Liberal, B. Grunenfelder, S. R. Chaves, C. H.
749 Spruck, S. I. Reed, H.-S. Martinsson-Ahlzén, V. Liberal, B. Grünenfelder, S. R.
750 Chaves, C. H. Spruck, S. I. Reed, Cyclin-dependent kinase-associated proteins
751 Cks1 and Cks2 are essential during early embryogenesis and for cell cycle
752 progression in somatic cells, *Mol Cell Biol* **28**, 5698–5709 (2008).
753 14. M. C. Morris, P. Kaiser, S. Rudyak, C. Baskerville, M. H. Watson, S. I. Reed,
754 Cks1-dependent proteasome recruitment and activation of CDC20 transcription in
755 budding yeast., *Nature* **423**, 1009–1013 (2003).
756 15. S. V Del Rincón, M. Widschwendter, D. Sun, S. Ekholm-Reed, J. Tat, L. K.
757 Teixeira, Z. Ellederova, E. Grolieres, S. I. Reed, C. Spruck, Cks overexpression
758 enhances chemotherapeutic efficacy by overriding DNA damage checkpoints.,
759 *Oncogene* , 1–7 (2014).
760 16. V. Liberal, H.-S. Martinsson-Ahlzén, J. Liberal, C. H. Spruck, M. Widschwendter,
761 C. H. McGowan, S. I. Reed, H. S. Martinsson-Ahlzen, J. Liberal, C. H. Spruck, M.
762 Widschwendter, C. H. McGowan, S. I. Reed, Cyclin-dependent kinase subunit (Cks)
763 1 or Cks2 overexpression overrides the DNA damage response barrier triggered by
764 activated oncoproteins., *Proc. Natl. Acad. Sci. U. S. A.* **109**, 2754–9 (2012).
765 17. C. Spruck, H. Strohmaier, M. Watson, A. P. L. Smith, A. Ryan, W. Krek, S. I.
766 Reed, A CDK-independent function of mammalian Cks1: Targeting of SCFSkp2 to
767 the CDK inhibitor p27Kip1, *Mol. Cell* **7**, 639–650 (2001).
768 18. A. Mocciaro, M. Rape, Emerging regulatory mechanisms in ubiquitindependent
769 cell cycle control*J. Cell Sci.* **125** (2012), doi:10.1242/jcs.091199.
770 19. A. Daulny, W. P. Tansey, Damage control: DNA repair, transcription, and the
771 ubiquitin-proteasome system*DNA Repair (Amst).* **8** (2009),
772 doi:10.1016/j.dnarep.2009.01.017.
773 20. A. V. Sorokin, A. A. Selyutina, M. A. Skabkin, S. G. Guryanov, I. V. Nazimov, C.
774 Richard, J. Th'Ng, J. Yau, P. H. B. Sorensen, L. P. Ovchinnikov, V. Evdokimova,
775 Proteasome-mediated cleavage of the Y-box-binding protein 1 is linked to DNA-
776 damage stress response, *EMBO J.* **24** (2005), doi:10.1038/sj.emboj.7600830.

777 21. X. Zhang, S. Linder, M. Bazzaro, Drug development targeting the ubiquitin-
778 proteasome system (UPS) for the treatment of human cancers*Cancers (Basel).* **12**
779 (2020), doi:10.3390/cancers12040902.
780 22. R. Aplenc, S. Meshinchi, L. Sung, T. Alonzo, J. Choi, B. Fisher, R. Gerbing, B.
781 Hirsch, T. Horton, S. Kahwash, J. Levine, M. Loken, L. Brodersen, J. Pollard, S.
782 Raimondi, E. A. Kolb, A. Gamis, Bortezomib with standard chemotherapy for children
783 with acute myeloid leukemia does not improve treatment outcomes: a report from the
784 Children's Oncology Group, *Haematologica* **105** (2020),
785 doi:10.3324/haematol.2019.220962.
786 23. R. T. Swords, S. Coutre, M. B. Maris, J. F. Zeidner, J. M. Foran, J. Cruz, H. P.
787 Erba, J. G. Berdeja, W. Tam, S. Vardhanabhuti, I. Pawlikowska-Dobler, H. M.
788 Faessel, A. B. Dash, F. Sedarati, B. J. Dezube, D. V. Faller, M. R. Savona,
789 Pevonedistat, a first-in-class NEDD8-activating enzyme (NAE) inhibitor, combined
790 with azacitidine, in patients with AML, *Blood* **228**, blood-2017-09-805895 (2018).
791 24. L. Zhou, S. Chen, Y. Zhang, M. Kmieciak, Y. Leng, L. Li, H. Lin, K. A. Rizzo, C. I.
792 Dumur, A. Ferreira-Gonzalez, M. Rahmani, L. Povirk, S. Chalasani, A. J. Berger, Y.
793 Dai, S. Grant, The NAE inhibitor pevonedistat interacts with the HDAC inhibitor
794 belinostat to target AML cells by disrupting the DDR., *Blood* **127**, 2219–30 (2016).
795 25. J. F. Zeidner, F. Mazerolle, J. A. Bell, L. E. Cain, D. V. Faller, M. Dalal, A.
796 Regnault, R. J. Fram, Randomized Phase 2 Trial of Pevonedistat Plus Azacitidine
797 Versus Azacitidine in Higher-Risk Myelodysplastic Syndromes/Chronic
798 Myelomonocytic Leukemia or Low-Blast Acute Myeloid Leukemia: Exploratory
799 Analysis of Patient-Reported Outcomes, *Blood* **136** (2020), doi:10.1182/blood-2020-
800 136935.
801 26. L. Wu, A. V Grigoryan, Y. Li, B. Hao, M. Pagano, T. J. Cardozo, Specific small
802 molecule inhibitors of Skp2-mediated p27 degradation., *Chem. Biol.* **19**, 1515–24
803 (2012).
804 27. S. C. Pavlides, K.-T. Huang, D. A. Reid, L. Wu, S. V Blank, K. Mittal, L. Guo, E.
805 Rothenberg, B. Rueda, T. Cardozo, L. I. Gold, Inhibitors of SCF-Skp2/Cks1 E3
806 ligase block estrogen-induced growth stimulation and degradation of nuclear
807 p27kip1: therapeutic potential for endometrial cancer., *Endocrinology* **154**, 4030–45
808 (2013).
809 28. D.-Y. Y. Shen, Z.-X. X. Fang, P. You, P.-G. G. Liu, F. Wang, C.-L. L. Huang, X.-
810 B. B. Yao, Z.-X. X. Chen, Z.-Y. Y. Zhang, Clinical significance and expression of

811 cyclin kinase subunits 1 and 2 in hepatocellular carcinoma, *Liver Int* **30**, 119–125
812 (2010).
813 29. S. Kitajima, Y. Kudo, I. Ogawa, T. Bashir, M. Kitagawa, M. Miyauchi, M. Pagano,
814 T. Takata, Role of Cks1 overexpression in oral squamous cell carcinomas:
815 cooperation with Skp2 in promoting p27 degradation., *Am. J. Pathol.* **165**, 2147–
816 2155 (2004).
817 30. T.-A. Masuda, H. Inoue, K. Nishida, H. Sonoda, Y. Yoshikawa, Y. Kakeji, T.
818 Utsunomiya, M. Mori, Cyclin-dependent kinase 1 gene expression is associated with
819 poor prognosis in gastric carcinoma., *Clin. Cancer Res.* **9**, 5693–5698 (2003).
820 31. P. Van Galen, V. Hovestadt, M. H. W. Ii, J. C. Aster, A. A. Lane, B. E. Bernstein,
821 P. Van Galen, V. Hovestadt, M. H. W. Ii, T. K. Hughes, G. K. Griffin, S. Battaglia, J.
822 A. Verga, J. Stephansky, T. J. Pastika, J. L. Story, Single-Cell RNA-Seq Reveals
823 AML Hierarchies Relevant to Disease Progression and Immunity Article Single-Cell
824 RNA-Seq Reveals AML Hierarchies Relevant to Disease Progression and Immunity,
825 *Cell* (2019).
826 32. B. de Boer, J. Prick, M. G. Pruis, P. Keane, M. R. Imperato, J. Jaques, A. Z.
827 Brouwers-Vos, S. M. Hogeling, C. M. Woolthuis, M. T. Nijk, A. Diepstra, S.
828 Wandinger, M. Versele, R. M. Attar, P. N. Cockerill, G. Huls, E. Vellenga, A. B.
829 Mulder, C. Bonifer, J. J. Schuringa, Prospective Isolation and Characterization of
830 Genetically and Functionally Distinct AML Subclones, *Cancer Cell* **34**, 674-689.e8
831 (2018).
832 33. M. Wunderlich, B. Mizukawa, F. S. Chou, C. Sexton, M. Shrestha, Y.
833 Saunthararajah, J. C. Mulloy, AML cells are differentially sensitive to chemotherapy
834 treatment in a human xenograft model, *Blood* (2013), doi:10.1182/blood-2012-10-
835 464677.
836 34. A. Camera, C. Andretta, M. R. Villa, M. Volpicelli, M. Picardi, M. Rossi, C. R.
837 Rinaldi, P. Della Cioppa, R. Ciancia, C. Selleri, B. Rotoli, Intestinal toxicity during
838 induction chemotherapy with cytarabine-based regimens in adult acute myeloid
839 leukemia, *Hematol. J.* (2003), doi:10.1038/sj.thj.6200304.
840 35. E. J. Bow, J. B. Meddings, Intestinal mucosal dysfunction and infection during
841 remission-induction therapy for acute myeloid leukaemia, *Leukemia* (2006),
842 doi:10.1038/sj.leu.2404440.
843 36. W. Grey, R. Chauhan, M. Piganeau, H. Huerga Encabo, M. Garcia-Albornoz, N.
844 Q. McDonald, D. Bonnet, Activation of the receptor tyrosine kinase, RET, improves

845 long-term hematopoietic stem cell outgrowth and potency, *Blood* (2020),
846 doi:10.1182/blood.2020006302.
847 37. A. Ludin, S. Gur-Cohen, K. Golan, K. B. Kaufmann, T. Itkin, C. Medaglia, X. J.
848 Lu, G. Ledergor, O. Kollet, T. Lapidot, Reactive oxygen species regulate
849 hematopoietic stem cell self-renewal, migration and development, as well as their
850 bone marrow microenvironment*Antioxidants Redox Signal.* (2014),
851 doi:10.1089/ars.2014.5941.
852 38. A. Kukalev, Y.-M. Ng, L. Ju, A. Saidi, S. Lane, A. Mondragon, D. Dormann, S. E.
853 Walker, W. Grey, P. W.-L. Ho, D. N. Stephens, A. M. Carr, K. Lamsa, E. Tse, V. P.
854 C. C. Yu, Deficiency of Cks1 Leads to Learning and Long-Term Memory Defects and
855 p27 Dependent Formation of Neuronal Cofilin Aggregates., *Cereb. Cortex* **27**, 11–23
856 (2017).
857 39. L. K. Nguyen, B. N. Kholodenko, A. von Kriegsheim, Rac1 and RhoA: Networks,
858 loops and bistability*Small GTPases* **9** (2018), doi:10.1080/21541248.2016.1224399.
859 40. F. Jiang, G. S. Liu, G. J. Dusting, E. C. Chan, NADPH oxidase-dependent redox
860 signaling in TGF-β-mediated fibrotic responses*Redox Biol.* (2014),
861 doi:10.1016/j.redox.2014.01.012.
862 41. E. D. Lagadinou, A. Sach, K. Callahan, R. M. Rossi, S. J. Neering, M.
863 Minhajuddin, J. M. Ashton, S. Pei, V. Grose, K. M. O'Dwyer, J. L. Liesveld, P. S.
864 Brookes, M. W. Becker, C. T. Jordan, BCL-2 inhibition targets oxidative
865 phosphorylation and selectively eradicates quiescent human leukemia stem cells,
866 *Cell Stem Cell* (2013), doi:10.1016/j.stem.2012.12.013.
867 42. A. Di Tullio, K. Rouault-Pierre, A. Abarrategi, S. Mian, W. Grey, J. Gribben, A.
868 Stewart, E. Blackwood, D. Bonnet, The combination of CHK1 inhibitor with G-CSF
869 overrides cytarabine resistance in human acute myeloid leukemia, *Nat. Commun.* **8**,
870 1679 (2017).
871 43. E. Batlle, H. Clevers, Cancer stem cells revisited*Nat. Med.* (2017),
872 doi:10.1038/nm.4409.
873 44. S. Raffel, D. Klimmeck, M. Falcone, A. Demir, A. Pouya, P. Zeisberger, C. Lutz,
874 M. Tinelli, O. Bischel, L. Bullinger, C. Thiede, A. Flörcken, J. Westermann, G.
875 Ehninger, A. D. Ho, C. Müller-Tidow, Z. Gu, C. Herrmann, J. Krijgsveld, A. Trumpp,
876 J. Hansson, Quantitative proteomics reveals specific metabolic features of Acute
877 Myeloid Leukemia stem cells, *Blood* (2020), doi:10.1182/blood.2019003654.
878 45. E. Aasebø, A. Brenner, F. Berven, Ø. Bruserud, F. Selheim, M. Hernandez-

879 Valladares, Proteomic Profiling of Primary Human Acute Myeloid Leukemia Cells
880 Does Not Reflect Their Constitutive Release of Soluble Mediators, *Proteomes* **7**, 1
881 (2018).
882 46. J. C. Mulloy, J. A. Cancelas, M. D. Filippi, T. A. Kalfa, F. Guo, Y. Zheng, Rho
883 GTPases in hematopoiesis and hemopathies*Blood* (2010), doi:10.1182/blood-2009-
884 09-198127.
885 47. M. del M. Maldonado, J. I. Medina, L. Velazquez, S. Dharmawardhane, Targeting
886 Rac and Cdc42 GEFs in Metastatic Cancer*Front. Cell Dev. Biol.* (2020),
887 doi:10.3389/fcell.2020.00201.
888 48. L. Shao, Y. Wang, J. Chang, Y. Luo, A. Meng, D. Zhou, Hematopoietic stem cell
889 senescence and cancer therapy-induced long-term bone marrow injury, *Transl.*
890 *Cancer Res.* (2013), doi:10.3978/j.issn.2218-676X.2013.10.05.
891 49. T. Cheng, N. Rodrigues, D. Dombkowski, S. Stier, D. T. Scadden, Stem cell
892 repopulation efficiency but not pool size is governed by p27(kip1)., *Nat. Med.* **6**,
893 1235–1240 (2000).
894 50. H. Kantarjian, S. O'Brisn, J. Cortes, F. Giles, S. Faderl, E. Jabbour, G. Garcia-
895 Manero, W. Wierda, S. Pierce, J. Shan, E. Estey, Results of intensive chemotherapy
896 in 998 patients age 65 years or older with acute myeloid leukemia or high-risk
897 myelodysplastic syndrome: Predictive prognostic models for outcome, *Cancer*
898 (2006), doi:10.1002/cncr.21723.
899 51. H. Kantarjian, F. Ravandi, S. O'Brien, J. Cortes, S. Faderl, G. Garcia-Manero, E.
900 Jabbour, W. Wierda, T. Kadia, S. Pierce, J. Shan, M. Keating, E. J. Freireich,
901 Intensive chemotherapy does not benefit most older patients (age 70 years or older)
902 with acute myeloid leukemia, *Blood* (2010), doi:10.1182/blood-2010-03-276485.
903 52. A. Batsivari, W. Grey, D. Bonnet, Understanding of the crosstalk between normal
904 residual hematopoietic stem cells and the leukemic niche in acute myeloid leukemia,
905 *Exp. Hematol.* (2021), doi:10.1016/j.exphem.2021.01.004.
906 53. A. Hamdi, A. Lesnard, P. Suzanne, T. Robert, M. a Miteva, M. Pellerano, B.
907 Didier, E. Ficko-Blean, A. Lobstein, M. Hibert, S. Rault, M. C. Morris, P. Colas,
908 Tampering with cell division by using small-molecule inhibitors of CDK-CKS protein
909 interactions., *Chembiochem* **16**, 432–9 (2015).
910 54. E. Griessinger, F. Anjos-Afonso, I. Pizzitola, K. Rouault-Pierre, J. Vargaftig, D.
911 Taussig, J. Gribben, F. Lassailly, D. Bonnet, A niche-like culture system allowing the
912 maintenance of primary human acute myeloid leukemia-initiating cells: a new tool to

913 decipher their chemoresistance and self-renewal mechanisms., *Stem Cells Transl.*
914 *Med.* **3**, 520–9 (2014).
915

916 **Figure Legends**

917 **Figure 1. Inhibition of CKS1-dependent protein degradation kills AML blast. A.**
918 Expression of *CKS1B* (relative to *GAPDH*) in a poor risk AML cohort. FAB and p53
919 status are indicated for each patient (FAB color coded, p53 status: white = WT; black
920 = mutant; *n*=32). **B.** Diagram of action for CKS1i binding and inhibition of the SCF^{SKP2-}
921 ^{CKS1} ubiquitin ligase complex. **C.** Correlation between CKS1i drug sensitivity (DSS)
922 and *CKS1B* expression (relative to *GAPDH*) **D.** Percentage of human $CD45^+$ cells of
923 total $CD45^+$ cells in mouse bone marrow aspirations one week after chemotherapy
924 (week 6). **E.** Correlation between *CKS1B* expression and reduction in human AML
925 burden post CKS1i treatment. **F-J.** Kaplan Meier plots and *P* value calculated (Mantel-
926 Cox test) for each individual PDX control and CKS1i treated cohort. Each data point
927 represents one mouse. A Student's *t*-test was used to calculate significance of
928 difference for all graphs unless otherwise stated. * $P<0.05$; ** $P<0.005$.

929

930

931 **Figure 2. AML LSCs have high CKS1 expression and are sensitive to CKS1i. A.**
932 *t*-stochastic neighbor embedding of patient AML7 illustrating co-expression of CKS1
933 protein with key LSC cell surface markers. **B.** Median intensity of CKS1 protein
934 abundance in bulk AML versus LSCs. **C.** Individual 1/L-LTC-IC frequencies with upper
935 and lower limits for each patient tested. Control (Grey) vs CKS1i (Blue). **D.** Fold
936 change L-LTC-IC frequency, CKS1i treatment versus control for all patient samples
937 tested. **E.** Overall survival of AML26 secondary transplantation with the indicated cell
938 doses from primary treatment mice. **F.** Estimated LSC frequency of secondary
939 transplanted AML26. Control calculated at week 6, CKS1i calculated at the end point
940 of the experiment. **G.** Percentage of apoptotic (Annexin V positive) LSCs in control
941 and CKS1i treated primary patient AML in vitro 24 hours after treatment. **H.**
942 Percentage of LSCs in total AML cells in control and CKS1i treated primary patient
943 AML in vitro 24 hours after treatment. A Student's *t*-test was used to calculate
944 significance of difference for all graphs unless otherwise stated. * $P<0.05$; ** $P<0.005$;
945 *** $P< 0.0005$.

946

947 **Figure 3. CKS1i protects normal hematopoietic cells from chemotherapeutic**
948 **toxicity by suppressing the cell cycle. A.** Percentage Annexin V positive apoptotic
949 cells for the indicated cell types in response to increasing concentrations of CKS1i. **B.**
950 p27 protein mean fluorescent intensity measured in $CD34^+$ cells cultured with CKS1i
951 (1μM) in the indicated cell populations. **C.** Cell cycle profile and **D.** Total cell count of
952 $CD34^+$ cells treated with the indicated doses of CKS1i (1μM for live cell count) for 24
953 hours. **E.** Illustration of $CD34^+$ engraftment and chemotherapeutic treatment in NSG
954 mice. **F.** Change in percentage human $CD45^+$ of total CD45 at the indicated time points
955 for Control (Ctrl), Doxorubicin/Cytarabine (DA) and Doxorubicin/Cytarabine plus
956 CKS1i (DAC) treatments. **G.** Fold change of the percentage of human CD45 cells at
957 week 4 and 6 for the indicated treatments (Control = Grey, DA = Green, DAC = Blue).
958 **H.** Representative flow plots and **I.** Percentage of total cells annexin V positive after 6
959 weeks in vivo for human CD45 cells with the indicated treatment conditions (Ctrl N=5,
960 DA N=3, DAC N=3). **J.** HSC frequency calculated by limiting dilution secondary
961 transplantation of human $CD45^+$ cells retrieved from primary mice (Control = Grey, DA
962 = Green, DAC = Blue). A Student's *t*-test was used to calculate significance of
963 difference unless otherwise stated. * $P<0.05$; ** $P<0.005$.
964
965
966 **Figure 4. CKS1i treatment induces divergent proteomic alterations in normal**
967 **and malignant hematopoietic cells. A.** Workflow for timescale of cell preparation for
968 mass spectrometry analysis. Volcano plots for proteomic alterations in **B.** THP-1 and
969 **C.** $CD34^+$ cells in response to CKS1i (1μM). **D.** Key differentially abundant proteins in
970 THP-1 or $CD34^+$ cells in response to CKS1i (n=4 per condition). **E.** Venn diagram
971 depicting overlap of differentially expressed proteins between THP-1 and $CD34^+$ cells.
972 **F.** Median expression of key intracellular signalling markers identified in CyTOF
973 analyses after CKS1i treatment (Ctrl n=3, CKS1i n=4). **G.** Representative flow plots
974 and quantified mean fluorescence intensity for non-phosphorylated β-catenin in $CD34^+$
975 cells grown for 48 hours in control conditions or treated with CKS1i (n=4). **H.**
976 Representative flow plots (including cells grown without OP-Puromycin; -OPP) and %
977 total OP-Puromycin incorporation in $CD34^+$ cells grown for 48 hours in control
978 conditions or treated with CKS1i. OP-Puromycin was added 1hr prior to collection and
979 fixation of cells (n=4). **I.** Representative flow plots and quantified mean fluorescence
980 intensity of intracellular reactive oxygen species (ROS) in $CD34^+$ cells grown for 48

981 hours in control conditions or treated with CKS1i (1μM) or NAC (1.25mM; *n*=3 per
982 condition). * *P*<0.05; ***P*<0.005; ****P*<0.0005; *****P*<0.0001.
983
984
985 **Figure 5. The SCF$^{SKP2-CKS1}$ complex controls RAC1/NADPH/ROS signalling. A.**
986 String network analysis of key differentially abundant proteins in THP-1 cells treated
987 with CKS1i. Red indicates upregulated, and blue indicates downregulated in response
988 to CKS1i treatment. **B.** RHOA-GTP and **C.** RAC1-GTP abundance in THP-1 cells
989 control or treated with CKS1i (1 μM) for 24 hours (*n*=3 independent experiments).
990 Total NADPH (pmol) in **D.** THP-1 and **E.** HL60 cells treated with the indicated doses
991 of CKS1i (+ = 1μM, ++ = 5μM) or NSC23766 (NSC; + = 0.1μM, ++ = 1μM) for 8 hours
992 (*n*=4 independent experiments per cell line and treatment). **F.** Representative flow
993 plots and **G.** Quantified mean fluorescence intensity of intracellular reactive oxygen
994 species (ROS) in the indicated cell lines in response to CKS1i (+ = 1μM) and NSC (+
995 = 0.1μM) treatment (*n*=3 per cell line and treatment). **H.** Representative flow plots and
996 **I-J.** Quantified mean fluorescence intensity of intracellular reactive oxygen species
997 (ROS) in the indicated cell lines in response to *CKS1B* knockdown and NSC (+ =
998 0.1μM) treatment (*n*=3 per cell line and treatment). **K-L.** Viability represented by
999 percentage reduction O_2 of the indicated cell lines in response to the indicated
1000 concentrations of CKS1i and NSC23766 (*n*=5 per cell line and treatment, except THP-
1001 1 where *n*=6), CKS1i (+ = 1μM) and NSC (+ = 0.1μM, ++ = 1μM). **M.** Percentage
1002 Annexin V positive apoptotic primary patient AML samples treated with the indicated
1003 doses of CKS1i (+ = 1μM) and NSC (+ = 0.1μM). **N.** Fold change cell number versus
1004 control for total AML (Blasts) and LSCs with the indicated treatments (CKS1i + = 1μM
1005 and NSC + = 0.1μM) 24 hours after treatment in vitro. A Student's *t*-test was used to
1006 calculate significance of difference for all graphs. * *P*<0.05; ***P*<0.005; *** *P*< 0.0005;
1007 **** *P*< 0.0001.
1008

1009 **Figure 6. CKS1i treatment depletes LSCs by inducing lethal ROS. A.**
1010 Representative flow plots and **B-C.** Quantified mean fluorescence intensity (MFI) of
1011 intracellular reactive oxygen species (ROS) in the indicated cell lines in response to
1012 CKS1i (+ = 1μM, ++ = 5μM) and NAC (+ = 1.25mM, ++ = 2.5mM) treatment (N=3 per
1013 cell line and treatment). **D-E.** Viability represented by percentage reduction O_2 of the
1014 indicated cell lines in response to the indicated concentrations of CKS1i (+ = 1μM, ++
1015 = 5μM) and NAC (+ = 1.25mM, ++ = 2.5mM; N=3 per cell line). Quantitative PCR
1016 analysis of *CDKN1A* expression in **F.** THP-1 cells treated with CKS1i, **G.** THP-1 cells
1017 with *CKS1B* knockdown, **H.** HL-60 cells treated with CKS1i and **I.** HL60 cells with
1018 *CKS1B* knockdown for 24 hours (*n*=3). **J.** Induction of apoptosis (Annexin V+) in
1019 primary patient LSCs in response to CKS1i and NAC (CKS1i + = 1μM, NAC + =
1020 1.25mM) 24 hours after treatment in vitro. **K.** Percentage LSCs of total primary patient
1021 AML blasts in response to CKS1i and NAC (CKS1i + = 1μM, NAC + = 1.25mM) 24
1022 hours after treatment in vitro. **L.** Fold change absolute number of primary patient LSCs
1023 in the indicated treatments versus control (CKS1i + = 1μM, CKS1i ++ = 5μM, NAC +
1024 = 1.25mM, NAC ++ = 2.5mM) 24 hours after treatment in vitro. A Student's *t*-test was
1025 used to calculate significance of difference for all graphs. * $P<0.05$; ** $P<0.005$; *** $P<$
1026 0.0005; **** $P<0.0001$.
1027

1028 **Figure 7. Combination of induction chemotherapy and CKS1i reduces AML**
1029 **burden and LSC potential whilst protecting resident hematopoietic cells. A.**
1030 *CKS1B* expression (relative to *GAPDH*) for patient AMLs tested in vivo. **B.** Percentage
1031 of human $CD45^+$ cells of total $CD45^+$ cells in mouse bone marrow aspirations one
1032 week after chemotherapy (week 6). **C.** Colony forming units per 10,000 mouse $CD45^+$
1033 cells extracted from week 6 bone marrow aspirations. **D.** Swimmer plots and *P* values
1034 calculated (Mantel-Cox test) for each individual PDX Control and treated mouse
1035 cohort. Each data point represents one mouse and days survived are presented.
1036 Treatment interval is illustrated as annotated. **E.** Total number of murine Long-term
1037 HSCs obtained from bone marrow of mice at the final survival time point (Ctrl *n*=8, DA
1038 *n*=5, DAC *n*=5). **F.** Serial colony forming units per 10,000 mouse $CD45^+$ cells obtained
1039 from BM of mice at the final survival time point (Ctrl *n*=6, DA *n*=5, DAC *n*=6). **G.** *CKS1B*
1040 expression (relative to *GAPDH*) for patient AMLs tested in L-LTC-IC. **H.** Fold change
1041 of live human $CD45^+$ cells, indicated treatments versus control, after two weeks of co-
1042 culture. **I.** Fold change of L-LTC-IC frequency of indicated treatment versus control,
1043 after 7 weeks of co-culture. **J-K.** LSC frequency in secondary transplanted mice
1044 injected with AML26 or AML32 at limiting dilutions 6 weeks post-transplantation. **L.**
1045 Kaplan-Meier survival curve for AML32 secondary mice up to 120 days. A Student's
1046 *t*-test was used to calculate significance of difference for all graphs unless otherwise
1047 stated. * $p<0.05$; ** $p<0.005$; *** $p< 0.0005$.

Figure 1.

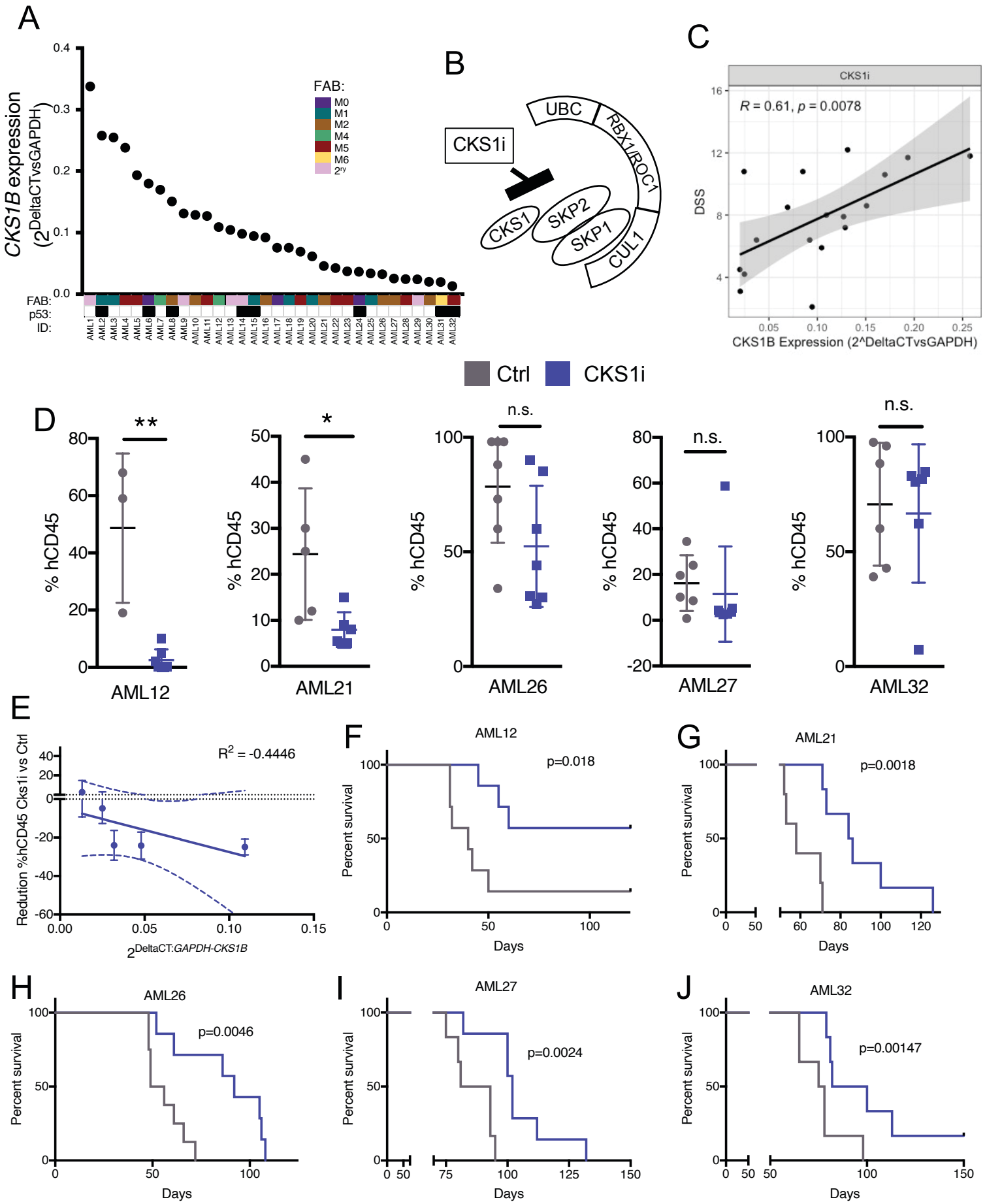
A
CKS1B expression (2DeltaCTvsGAPDH)
FAB:
M0
M1
M2
M4
M5
M6
2ry
p53:
ID:
B
CKS1i
UBC
RBX1/ROC1
CKS1
SKP2
SKP1
CUL1
C
CKS1i
R = 0.61, p = 0.0078
DSS
CKS1B Expression (2^DeltaCTvsGAPDH)
Ctrl
CKS1i
D
% hCD45
AML12
AML21
AML26
AML27
AML32
n.s.
E
R2 = -0.4446
Redution %hCD45 Cks1i vs Ctrl
2DeltaCT:GAPDH-CKS1B
F
AML12
p=0.018
Percent survival
Days
G
AML21
p=0.0018
H
AML26
p=0.0046
I
AML27
p=0.0024
J
AML32
p=0.00147

Figure 2.

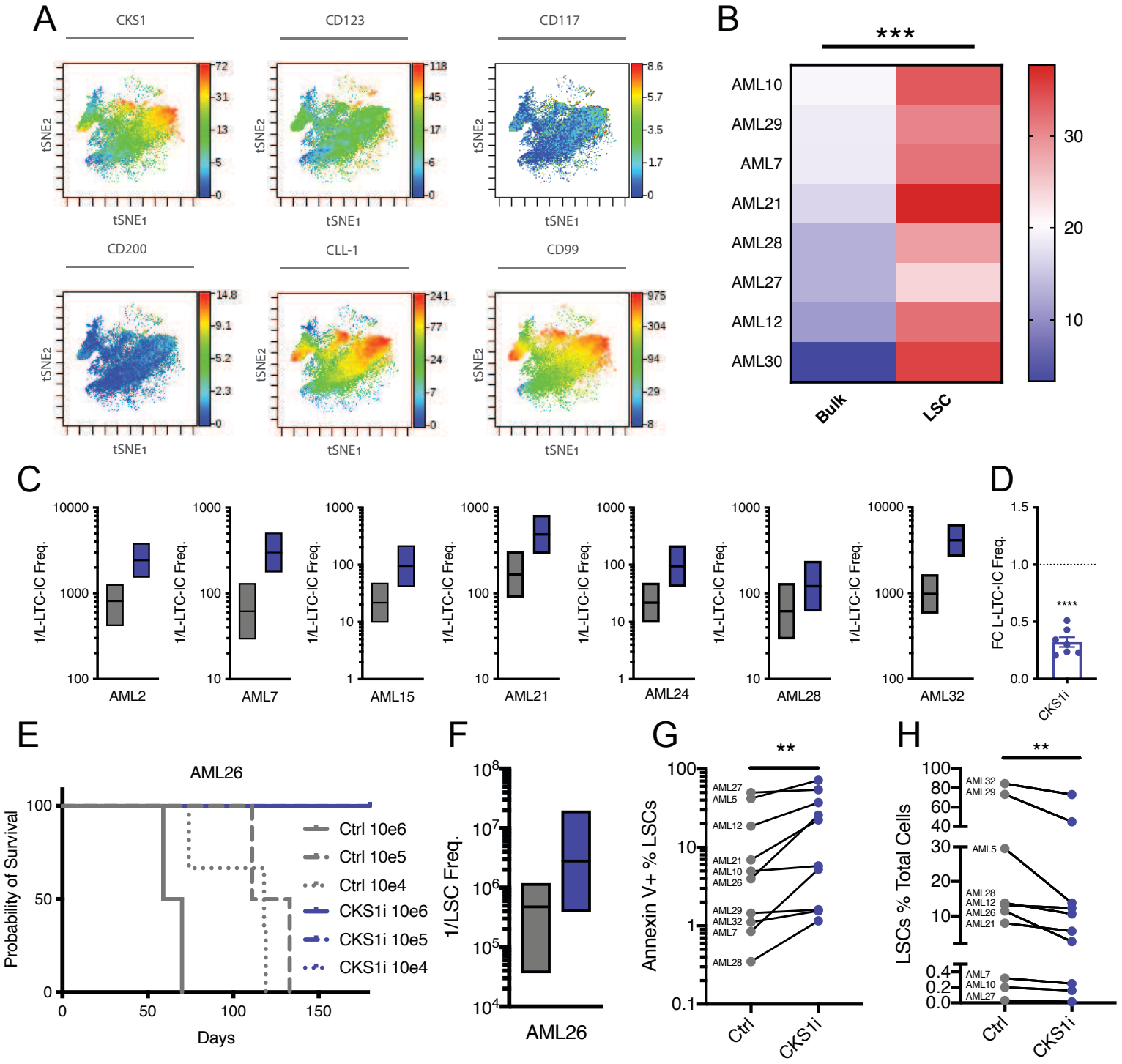
A
CKS1
CD123
CD117
CD200
CLL-1
CD99
tSNE1
tSNE2
B
***
AML10
AML29
AML7
AML21
AML28
AML27
AML12
AML30
Bulk
LSC
C
1/L-LTC-IC Freq.
AML2
AML7
AML15
AML21
AML24
AML28
AML32
D
FC L-LTC-IC Freq.
****
CKS1i
E
AML26
Probability of Survival
Days
Ctrl 10e6
Ctrl 10e5
Ctrl 10e4
CKS1i 10e6
CKS1i 10e5
CKS1i 10e4
F
1/LSC Freq.
AML26
G
**
Annexin V+ % LSCs
Ctrl
CKS1i
H
**
LSCs % Total Cells
Ctrl
CKS1i

Figure 3.

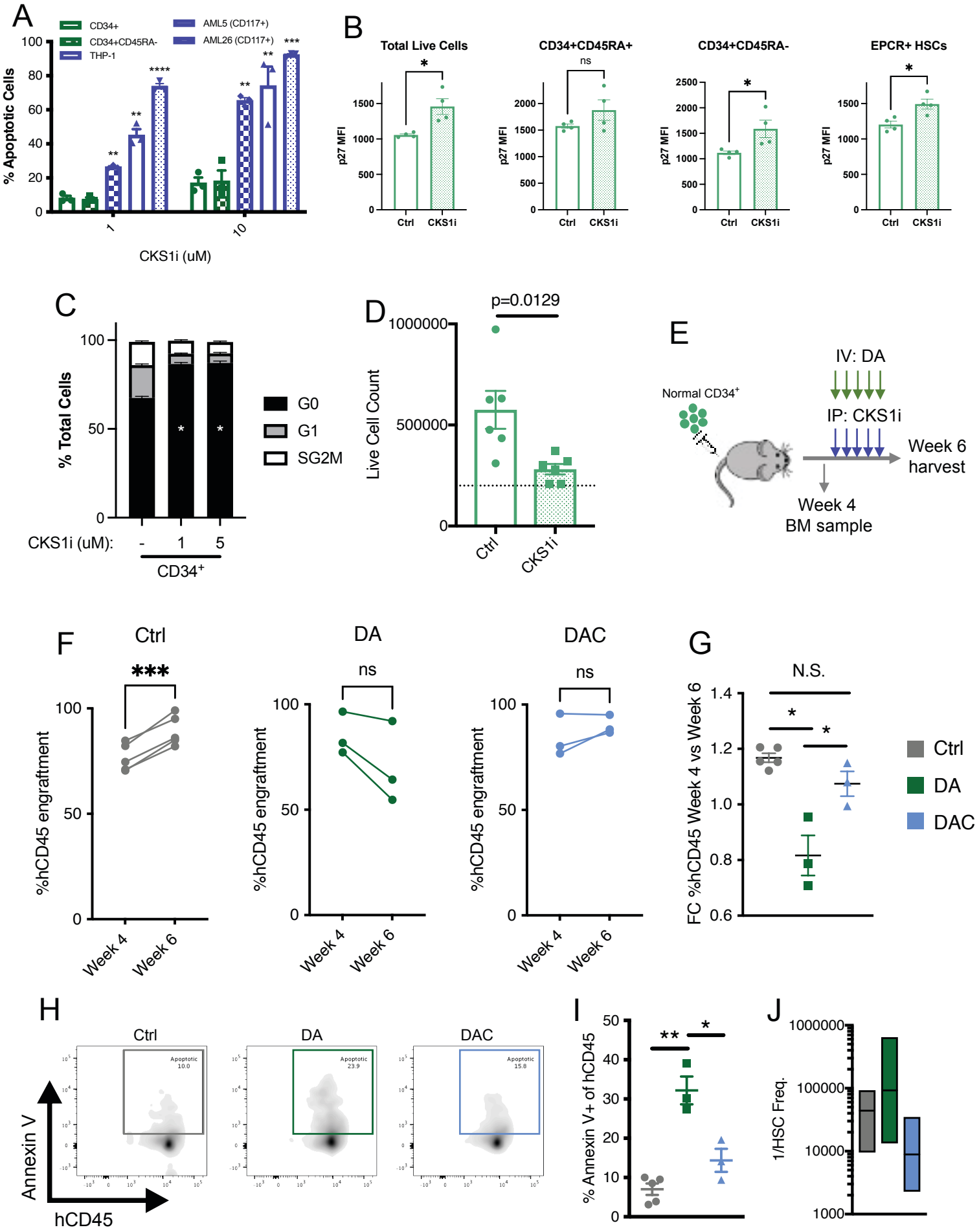
A
CD34+
CD34+CD45RA-
THP-1
AML5 (CD117+)
AML26 (CD117+)
% Apoptotic Cells
CKS1i (uM)
B
Total Live Cells
CD34+CD45RA+
CD34+CD45RA-
EPCR+ HSCs
p27 MFI
Ctrl
CKS1i
C
% Total Cells
G0
G1
SG2M
CKS1i (uM):
CD34+
D
p=0.0129
Live Cell Count
E
Normal CD34+
IV: DA
IP: CKS1i
Week 6 harvest
Week 4 BM sample
F
Ctrl
DA
DAC
ns
%hCD45 engraftment
Week 4
Week 6
G
N.S.
FC %hCD45 Week 4 vs Week 6
H
Apoptotic 10.0
Apoptotic 23.9
Apoptotic 15.8
Annexin V
hCD45
I
% Annexin V+ of hCD45
J
1/HSC Freq.

Figure 4.

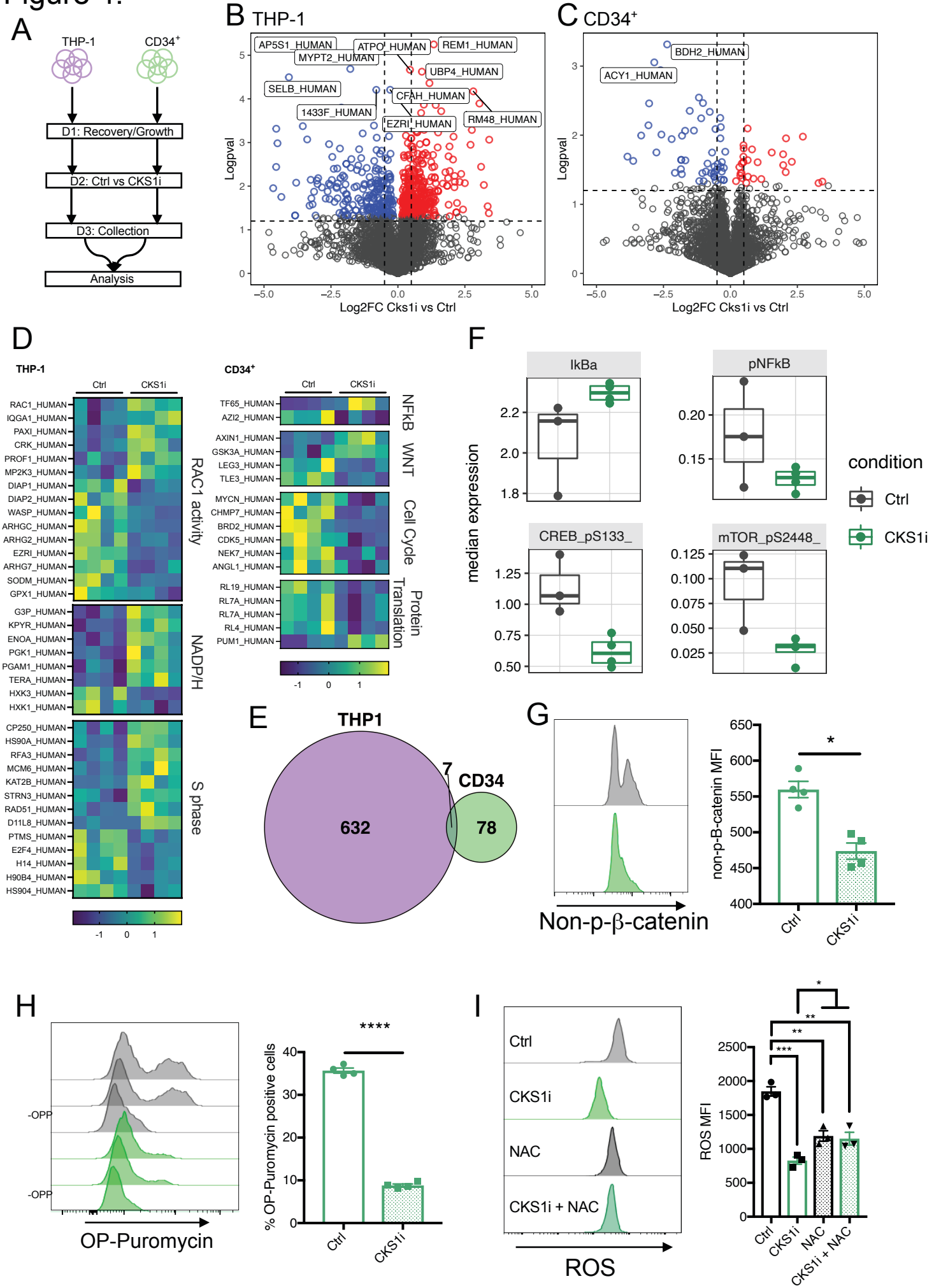
A
THP-1
CD34+
D1: Recovery/Growth
D2: Ctrl vs CKS1i
D3: Collection
Analysis
B THP-1
AP5S1_HUMAN
MYPT2_HUMAN
ATPO_HUMAN
REM1_HUMAN
UBP4_HUMAN
SELB_HUMAN
CFAH_HUMAN
1433F_HUMAN
EZRI_HUMAN
RM48_HUMAN
Logpval
Log2FC Cks1i vs Ctrl
C CD34+
BDH2_HUMAN
ACY1_HUMAN
Logpval
Log2FC Cks1i vs Ctrl
D
THP-1
CD34+
Ctrl
CKS1i
RAC1 activity
NADP/H
S phase
NFkB
WNT
Cell Cycle
Protein Translation
F
IkBa
pNFkB
CREB_pS133_
mTOR_pS2448_
median expression
condition
Ctrl
CKS1i
E
THP1
CD34
632
7
78
G
Non-p-β-catenin
non-p-B-catenin MFI
Ctrl
CKS1i
H
-OPP
OP-Puromycin
% OP-Puromycin positive cells
Ctrl
CKS1i
I
Ctrl
CKS1i
NAC
CKS1i + NAC
ROS
ROS MFI
Ctrl
CKS1i
NAC
CKS1i + NAC

Figure 5.

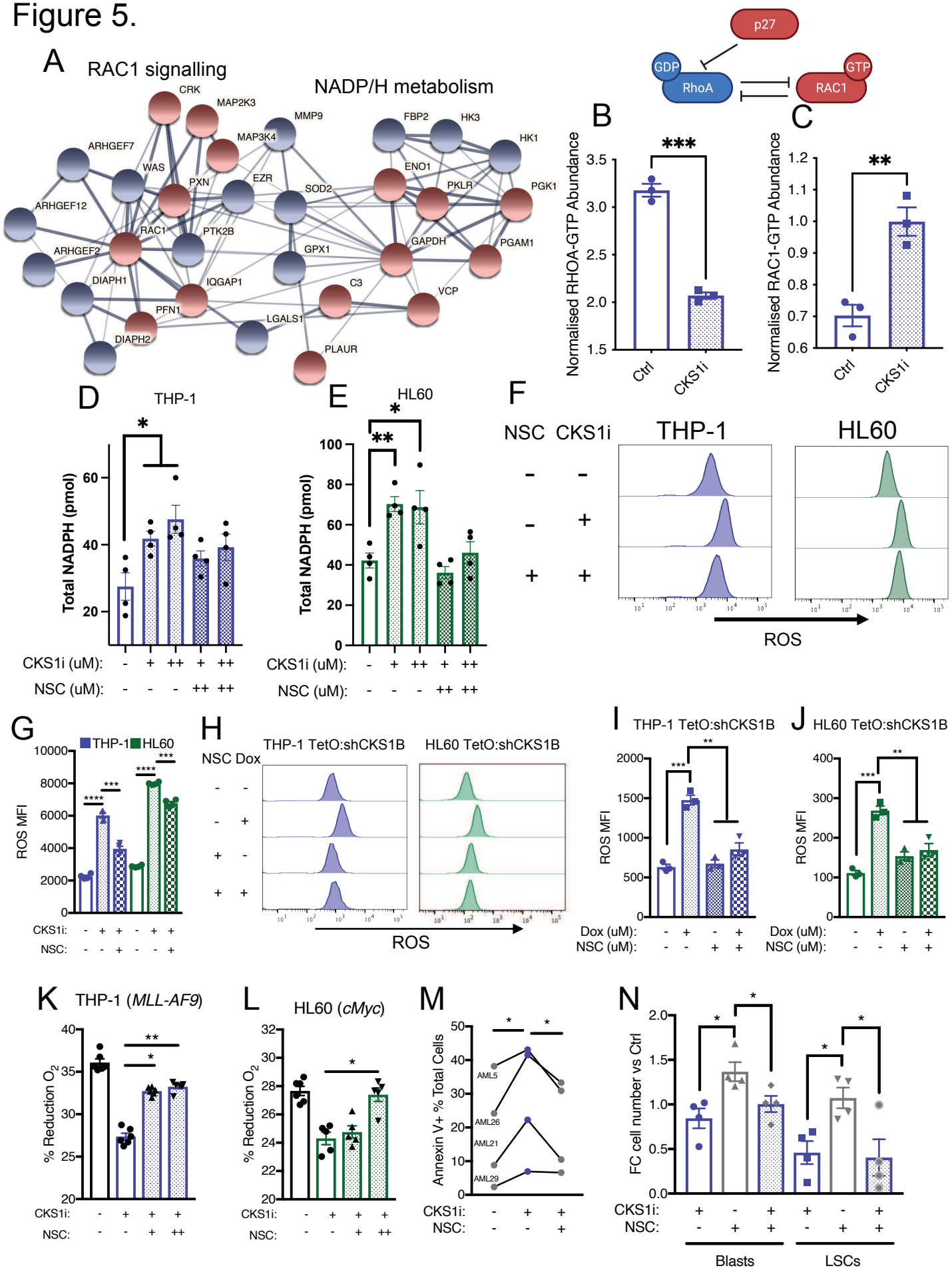
A
RAC1 signalling
NADP/H metabolism
CRK
MAP2K3
MMP9
FBP2
HK3
HK1
ARHGEF7
MAP3K4
WAS
PXN
EZR
SOD2
ENO1
PKLR
PGK1
ARHGEF12
RAC1
PTK2B
GPX1
GAPDH
PGAM1
ARHGEF2
DIAPH1
IQGAP1
C3
VCP
PFN1
LGALS1
DIAPH2
PLAUR
p27
GDP
RhoA
GTP
RAC1
B
Normalised RHOA-GTP Abundance
***
Ctrl
CKS1i
C
Normalised RAC1-GTP Abundance
**
Ctrl
CKS1i
D
THP-1
Total NADPH (pmol)
CKS1i (uM):
NSC (uM):
E
HL60
Total NADPH (pmol)
CKS1i (uM):
NSC (uM):
F
NSC CKS1i
THP-1
HL60
ROS
G
THP-1 HL60
ROS MFI
CKS1i:
NSC:
H
NSC Dox
THP-1 TetO:shCKS1B
HL60 TetO:shCKS1B
ROS
I
THP-1 TetO:shCKS1B
ROS MFI
Dox (uM):
NSC (uM):
J
HL60 TetO:shCKS1B
ROS MFI
Dox (uM):
NSC (uM):
K
THP-1 (MLL-AF9)
% Reduction O2
CKS1i:
NSC:
L
HL60 (cMyc)
% Reduction O2
CKS1i:
NSC:
M
Annexin V+ % Total Cells
AML5
AML26
AML21
AML29
CKS1i:
NSC:
N
FC cell number vs Ctrl
CKS1i:
NSC:
Blasts
LSCs

Figure 6.

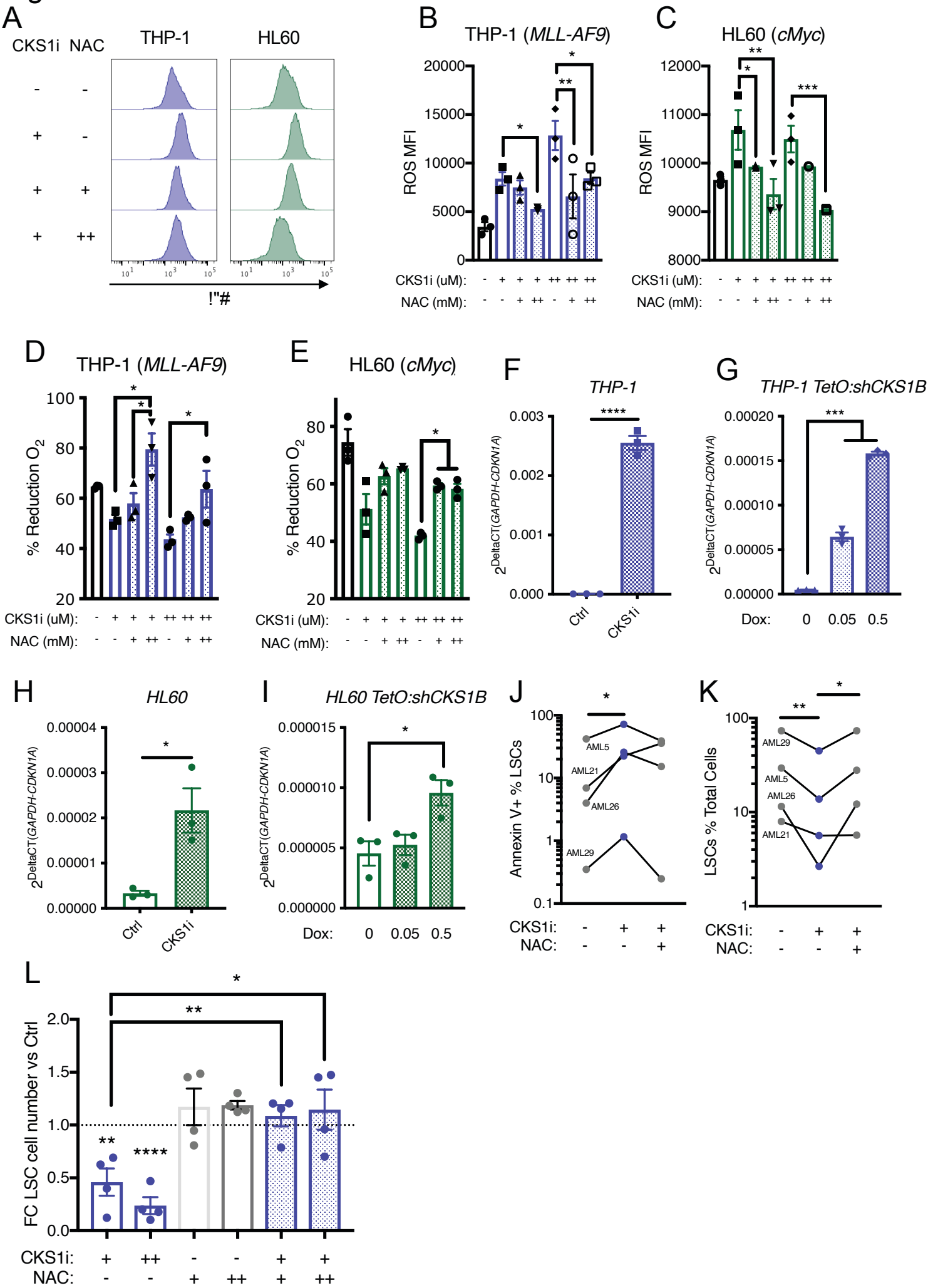
A
CKS1i NAC
THP-1
HL60
!"#
B
THP-1 (MLL-AF9)
ROS MFI
CKS1i (uM):
NAC (mM):
C
HL60 (cMyc)
ROS MFI
D
THP-1 (MLL-AF9)
% Reduction O2
E
HL60 (cMyc)
% Reduction O2
F
THP-1
2DeltaCT(GAPDH-CDKN1A)
Ctrl
CKS1i
G
THP-1 TetO:shCKS1B
Dox:
H
HL60
I
HL60 TetO:shCKS1B
J
Annexin V+ % LSCs
AML5
AML21
AML26
AML29
K
LSCs % Total Cells
L
FC LSC cell number vs Ctrl

Figure 7.

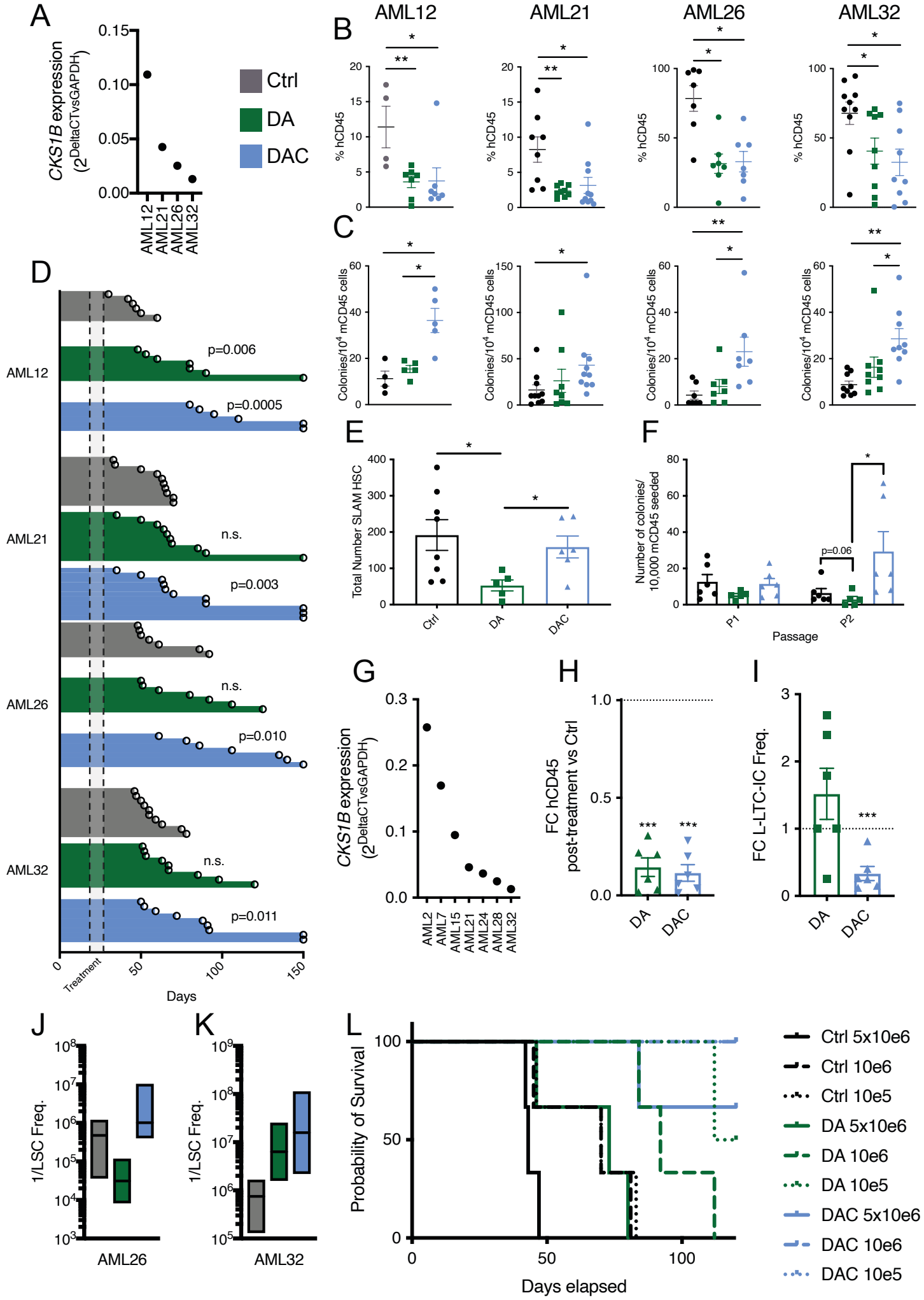
A
CKS1B expression (2^DeltaCTvsGAPDH)
0.15
0.10
0.05
0.00
AML12
AML21
AML26
AML32
Ctrl
DA
DAC
B
AML12
AML21
AML26
AML32
% hCD45
C
Colonies/10^4 mCD45 cells
D
AML12
AML21
AML26
AML32
p=0.006
p=0.0005
n.s.
p=0.003
n.s.
p=0.010
n.s.
p=0.011
Treatment
Days
E
Total Number SLAM HSC
Ctrl
DA
DAC
F
Number of colonies/ 10,000 mCD45 seeded
p=0.06
P1
P2
Passage
G
CKS1B expression (2^DeltaCTvsGAPDH)
AML2
AML7
AML15
AML21
AML24
AML28
AML32
H
FC hCD45 post-treatment vs Ctrl
DA
DAC
I
FC L-LTC-IC Freq.
DA
DAC
J
1/LSC Freq.
AML26
K
1/LSC Freq.
AML32
L
Probability of Survival
Days elapsed
Ctrl 5x10e6
Ctrl 10e6
Ctrl 10e5
DA 5x10e6
DA 10e6
DA 10e5
DAC 5x10e6
DAC 10e6
DAC 10e5

Supplementary Information

Supplementary Methods

AML cell line, AML primary sample, UCB $CD34^+$ and MS-5 culture

All AML cell lines and MS-5 stromal cells were originally obtained from the ATCC and maintained by the Francis Crick Cell Services. Before using these lines, they were authenticated using the Short Tandem Repeat (SRF) profiling and tested for mycoplasma prior to commencing experiments. All AML cell lines were cultured in RPMI 1640, 10% heat-inactivated FBS and 1% penicillin/streptomycin (Life Technologies) at 37ºC, 5% CO_2. Umbilical cord blood $CD34^+$ cells were cultured in StemSpan SFEMMII (StemCell Technologies) supplemented with Human SCF (150ng/ml), Human FLT3 ligand (150ng/ml) and Human TPO (20ng/ml; all Peprotech) at $2x10^5$ cells/ml at 37ºC, 5% CO_2. For relative viability, apoptosis and IC_{50} calculations cell lines were seeded in 96 well plates at a concentration of $2x10^5$ cells/ml with the indicated dose of drug. Measurements of viability (% reduction O_2) or apoptosis (Annexin V positivity) were taken at 48 hours post-treatment. MS-5 stromal cells were cultured in IMDM, 10% heat-inactivated FBS and 2% penicillin/streptomycin (Life Technologies) at 37ºC, 5% CO_2. Primary human AML samples were recovered for 24 hours in StemSpan SFEMMII (Stem Cell Technologies) supplemented with IL-3, G-CSF, TPO (20ng/ml each; all Peprotech) and treated as indicated.

Mass Spectrometry

THP-1 AML cell lines and UCB $CD34^+$ cells were cultured as per culture and drug treatment in methods. Cells were recovered for 24 hours in their respective media followed by sub-lethal AML doses of CKS1i (1μM) for 12 hours. All cells were retrieved from wells, washed three times in ice-cold PBS and snap frozen in liquid nitrogen as dry pellets. Cells were cultured in the conditions above, with differing media compositions.

Cell pellets were lysed in 100 μL of urea buffer (8 M urea in 20 mM HEPES, pH: 8.0), lysates were further homogenized by sonication (30 cycles of 30s on 30s off; Diagenode Bioruptor Plus) and insoluble material was removed by centrifugation. Protein amount was quantified using BCA (Thermo Fisher Scientific). Then, 100 and 20 μg of protein for THP-1 and $CD34^+$ samples, respectively, were diluted in urea

35 buffer to a final volume of 300 μL and subjected to cysteine alkylation using sequential
36 incubation with 10 mM dithiothreitol (DDT) and 16.6 mM iodoacetamide (IAM) for 1 h
37 and 30 min, respectively, at 25 °C with agitation. Trypsin beads (50% slurry of TLCK-
38 trypsin; Thermo-Fisher Scientific; Cat. #20230) were equilibrated with 3 washes with
39 20 mM HEPES (pH 8.0), the urea concentration in the protein suspensions was
40 reduced to 2 M by the addition of 900 μL of 20 mM HEPES (pH 8.0), 100 μL of
41 equilibrated trypsin beads were added and samples were incubated overnight at 37°C.
42 Trypsin beads were removed by centrifugation (2000 xg at 5°C for 5 min) and the
43 resulting peptide solutions were desalted using carbon C18 spin tips (Glygen; Cat. #
44 TT2MC18). Briefly, spin tips were activated twice with 200 μL of Elution Solution (70%
45 ACN, 0.1% TFA) and equilibrated twice with 200 μL of Wash Solution (1% ACN, 0.1%
46 TFA). Samples were loaded and spin tips were washed twice with 200 μL of Wash
47 Solution. Peptides were eluted into fresh tubes from the spin tips with 4 times with 50
48 μl of Elution Solution. In each of the desalting steps, spin tips were centrifuged at
49 1,500xg at 5C for 3 min. Finally, samples were dried in a SpeedVac and peptide pellets
50 were stored at −80°C.
51 For mass spectrometry identification and quantification of proteins, samples were run
52 twice in a LC-MS/MS platform. Briefly, peptide pellets were resuspended in 100 μL
53 and 20 μL of reconstitution buffer (20 fmol/μL enolase in 3% ACN, 0.1% TFA) for THP-
54 1 and $CD34^+$ samples, respectively. Then, 2 μL were loaded onto an LC-MS/MS
55 system consisting of a Dionex UltiMate 3000 RSLC coupled to a Q Exactive Plus
56 Orbitrap Mass Spectrometer (Thermo Fisher Scientific) through an EASY-Spray
57 source (Cat. # ES081, Thermo Fisher Scientific). Mobile phases for the
58 chromatographic separation of the peptides consisted in Solvent A (3% ACN: 0.1%
59 FA) and Solvent B (99.9% ACN; 0.1% FA). Peptides were loaded in a micro-pre-
60 column (Acclaim PepMap 100 C18 LC; Cat. # 160454, Thermo Fisher Scientific) and
61 separated in an analytical column (Acclaim PepMap 100 C18 LC; Cat. # 164569,
62 Thermo Fisher Scientific) using a gradient running from 3% to 23% over 120 min. The
63 UPLC system delivered a flow of 2 μL/min (loading) and 300 nL/min (gradient elution).
64 The Q-Exactive Plus operated a duty cycle of 2.1s. Thus, it acquired full scan survey
65 spectra (m/z 375–1500) with a 70,000 FWHM resolution followed by data-dependent
66 acquisition in which the 15 most intense ions were selected for HCD (higher energy
67 collisional dissociation) and MS/MS scanning (200–2000 m/z) with a resolution of

17,500 FWHM. A dynamic exclusion period of 30s was enabled with a m/z window of ±10 ppms.

Peptide identification from MS data was automated using a Mascot Daemon 2.5.0 workflow in which Mascot Distiller v2.5.1.0 generated peak list files (MGFs) from RAW data and the Mascot search engine (v2.5) matched the MS/MS data stored in the MGF files to peptides using the SwissProt Database (SwissProt_2016Oct.fasta). Searches had a FDR of ~1% and allowed 2 trypsin missed cleavages, mass tolerance of ±10 ppm for the MS scans and ±25 mmu for the MS/MS scans, carbamidomethyl Cys as a fixed modification and PyroGlu on N-terminal Gln and oxidation of Met as variable modifications. Identified peptides were quantified using Pescal software in a label free procedure based on extracted ion chromatograms (XICs). Thus, the software constructed XICs for all the peptides identified across all samples with mass and retention time windows of ±7 ppm and ±2 min, respectively and calculated the area under the peak. Individual peptide intensity values in each sample were normalized to the sum of the intensity values of all the peptides quantified in that sample. Data points not quantified were given a peptide intensity value equal to the minimum intensity value quantified in the sample divided by 10. Protein intensity values were calculated by adding the individual normalized intensities of all the peptides comprised in a protein and values of 2 technical replicates per sample were averaged. Protein score values were expressed as the maximum Mascot protein score value obtained across samples.

<u>Drug sensitivity and resistance testing (DSRT)</u>

Single drug DSRT was performed as described previously*(52)*. In brief, compounds, each with 7 different concentrations, were pre-plated using an acoustic liquid handling Echo 550 (Labcyte) to 384-well plates. Primary AML cells were suspended in conditioned medium (RPMI 1640 supplemented with 10% fetal bovine serum, 2mM L-glutamine, penicillin-100U/ml, streptomucing-100ug/ml and 12.5% conditioned medium from HS-5 human bone marrow stromal cells), DNase I treated for 4h (Promega), filtered through a 70μm cell strainer (Thermo Fisher Scientific) to remove possible cell clumps, and viable cells were counted. Pre-plated compounds in each 384-well plate were dissolved in 5ul of conditioned medium using a MultiDrop Combi peristaltic dispenser (Thermo Fisher Scientific) and shaken for 5 minutes to dissolve

102 the compounds. AML cells were plated at 5,000 cells/well in 20ul, leading to a final
103 volume of 25ul/well. Plates were gently shaken for 5 minutes to mix the cells with the
104 compounds and incubated for 72 hours at 37ºC, 5% CO_2.
105 Cell viability was measured using the CellTiter-Glo assay (Promega) with a
106 PHERAstar microplate reader (BMG-labtech). Data was normalised to negative
107 (DMSO only) and positive control wells (100uM benzethonium chloride) and dose
108 response curves calculated.
109 *Ex vivo* drug sensitivity of AML cells to the tested drugs was calculated using a drug
110 sensitivity score (DSS), a modified form of the area under the inhibition curve
111 calculation that integrates multiple dose response parameters for each of the tested
112 drugs, as previously described*(53)*.
113
114 Intestinal crypt analyses
115 Tamoxifen (Sigma, #T5648) was dissolved in ethanol to 300 mg/ml and further diluted
116 in sunflower seed oil (Sigma #S5007) to a final concentration of 30 mg/ml. To induce
117 recombination, 6-14 weeks old $Lgr5^{tm1(cre/ERT2)Cle}$ mice were given one dose of
118 tamoxifen (150 ug/g body weight) via oral gavage. After 24h, chemotherapy was
119 administered as described above. After seven days the animals were culled, the
120 intestines harvested and fixed in 10% neutral buffered formalin for 24h and
121 subsequently transferred to 70% ethanol. After embedding and sectioning, the slides
122 were stained with anti-EGFP (LGR5) or Ki67 and the number of positive crypts (LGR5)
123 or cells per crypt (Ki67) were counted.
124
125 AML cell line in vivo experimentation
126 AML cell lines were transduced with GFP-Luciferase containing vectors as per our
127 previous reports *(41)*. For both cell lines (THP-1 and HL60) $2x10^6$ cells were injected
128 I.V. into unconditioned 10-12 weeks old female or male NSG mice. After 7 days
129 engraftment was assessed by bioluminescence imaging. Isofluorane anesthetized
130 mice were imaged 5-10 minutes post D-luciferin injection I.P. (15mg.kg; Caliper life
131 sciences) using the Xenogen IVIS imaging system. Photons emitted were expressed
132 as Flux (photons/s/cm^2), and quantified and analysed using “living image” software
133 (Caliper life sciences).
134
135

136 Colony forming units

137 For resident mouse hematopoietic cell response to 5-FU', CKS1i, DA and DAC, colony
138 forming ability was assessed in methylcellulose (StemCell Technologies M3434-GF).
139 10^4 mCD45$^+$ cells were sorted from PDX mice at the indicated points and seeded in
140 methylcellulose and scored to colony forming units after 7 days. Cultures were
141 dissolved in PBS, counted and 10^4 cells were re-seeded for passage 2 and passage
142 3.

143

144 Viability assays

145 Relative cell viability was assessed by % reduction O_2 in culture wells using the Alamar
146 blue cell viability reagent (Life Technologies). Cells were seeded in 96 well plates at
147 $2x10^5$ cells/ml and the indicated dose of drugs were added on top and incubated for
148 48 hours. Alamar blue reagent was added on top of cells, and cells were incubated for
149 another 4 hours under the same conditions (37ºC, 5% CO_2). Plates were read on a
150 spectramax plate reader (Biostars) at 570nm and 600nm and % reduction O_2 was
151 calculated as per the manufacturer's instructions.

152

153 Flow Cytometry, apoptosis and cell cycle assays

154 Flow cytometry analysis was performed using a BD Fortessa flow cytometer (BD
155 biosciences). Cells were prepared by washing in PBS + 1% FBS three times before
156 staining in the same media with the indicated cell surface antibodies (resources table)
157 for 1 hour at 4C. For apoptosis assays, cells were incubated with annexin V binding
158 buffer in addition to the washing media (BD biosciences), washed three times in PBS
159 + 1% FBS + 1x annexin V binding buffer and incubated with 0.1μg/ml DAPI prior to
160 flow cytometry analysis. For cell cycle analysis, cells were washed three times in PBS
161 + 1% FBS and fixed in BD fix/perm buffer (BD biosciences) for 20 minutes at room
162 temperature. Cells were washed three times in BD perm/wash buffer + 0.1% Triton X-
163 100 (BD biosciences) and incubated with intracellular antibodies, such as anti-Ki67,
164 for 4 hours at 4C. Cells were washed three times in BD perm/wash buffer and 0.5
165 μg/ml DAPI was added for 15 minutes prior to analysis. For all flow cytometry, cells
166 were initially identified based on forward and side scatter.

167
168
169

170 RNA extraction, reverse transcription and real time quantitative PCR (RT-qPCR)
171 Total RNA was isolated from patient samples after thawing, density centrifugation and
172 T-cell depletion, using a RNeasy mini kit (Qiagen). Resulting RNA was reverse
173 transcribed to produce cDNA using the Superscript III reverse transcriptase kit
174 (Thermo Fisher Scientific) with oligoDT_{20} primers (Sigma Aldrich). RT-qPCR
175 experiments were performed with an ABI-7500 FAST Thermal Cycler (Applied
176 Biosystems) using SYBR Green (Thermo Fisher Scientific). RNA abundance was
177 quantified by the Comparative CT method with two independent control genes
178 (*GAPDH* and *B-ACTIN*, *GAPDH* presented). The CT values used for each patient
179 sample were the result of three technical triplicates. Primers are described in the
180 resources table.
181
182 RAC1/RHOA G-LISA assay
183 Analysis of RAC1/RHOA-GTP abundance was carried out using the RAC1/RHOA G-
184 LISA assay as per the manufacturer's instructions (Cytoskeleton inc.). Control and
185 CKS1i treated AML cells were lysed on ice with the provided lysis buffer for 10 minutes
186 and centrifuged at 10,000g, 4°C, for 5 minutes. Protein was quantified and normalized
187 with precision red protein reagent. Lysate, lysis buffer only or control protein was
188 incubated with G-LISA wells at 4°C for 30 minutes with agitation. Wells were washed
189 three times with wash buffer and primary antibody incubation was carried out at room
190 temperature for 45 minutes with agitation. Wells were washed three times with wash
191 buffer and secondary antibody incubation was carried out at room temperature for a
192 further 45 minutes with agitation. HRP detection reagent was added to each well and
193 incubated at room temperature for 20 minutes (RAC1) or 15 minutes at 37C (RHOA)
194 in the dark followed by measurement at 490nm.

Supplementary Figures

Supplementary Figure 1.

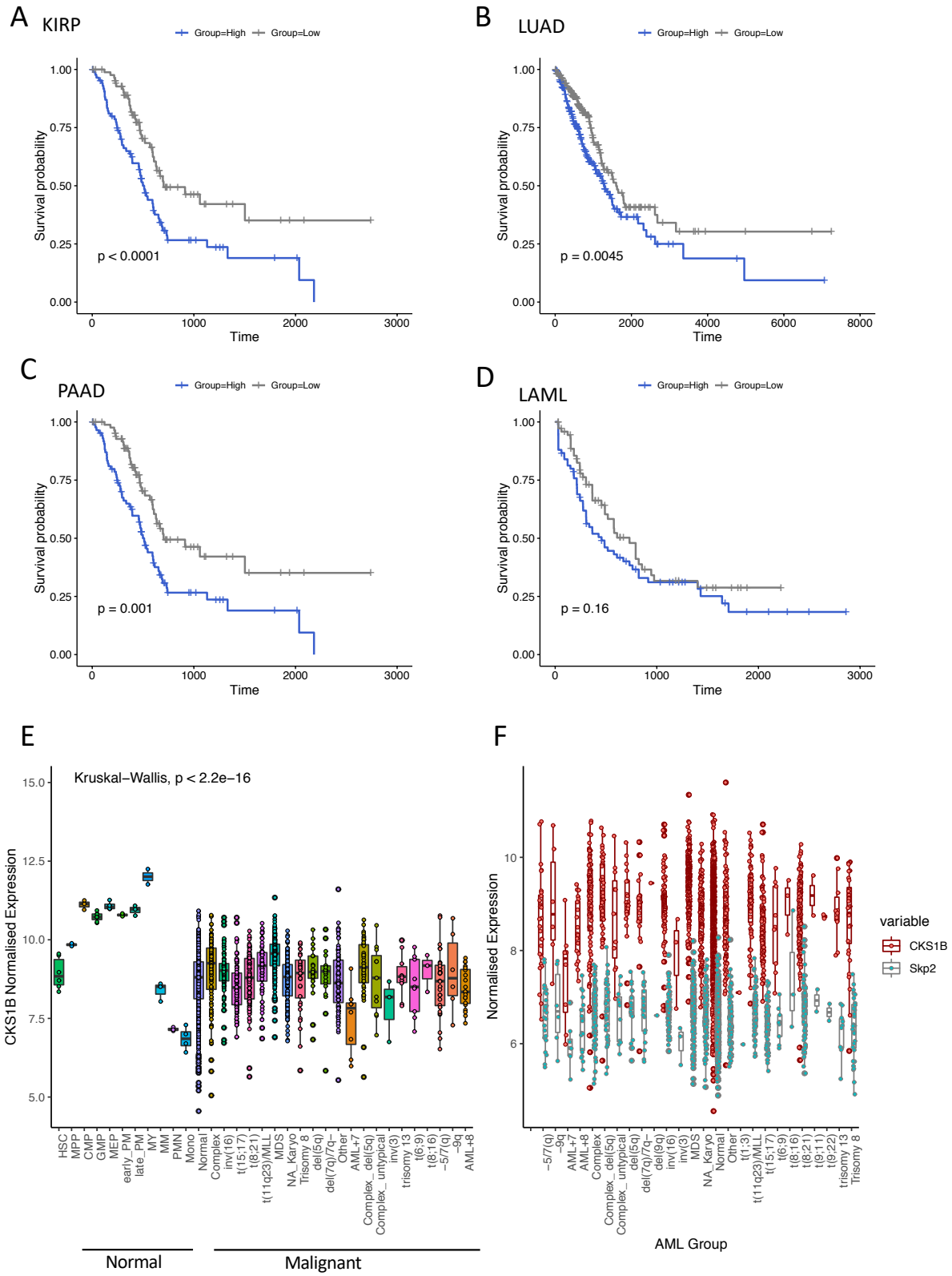

198 **Supplementary Figure 1. Expression of *CKS1B* across publicly available**
199 **datasets. A-D.** Overall survival of TCGA patients stratified for *CKS1B* expression (50th
200 percentile). Cohorts are as follows: KIRP = Kidney Renal Papillary Cell Carcinoma,
201 LUAD = Lung Adenocarcinoma, PAAD = Pancreatic Adenocarcinoma, LAML = Acute
202 Myeloid Leukemia. **E** *CKS1B* normalized expression and **F.** *SKP2* compared to
203 *CKS1B* normalized expression of normal and malignant hematopoeitic cells obtained
204 from Bloodspot.eu. Data sources: Human normal hematopoiesis (GSE42519), Human
205 AML (GSE13159, GSE15434, GSE61804, GSE14468 and The Cancer Genome
206 Atlas; TCGA).

Supplementary Figure 2.

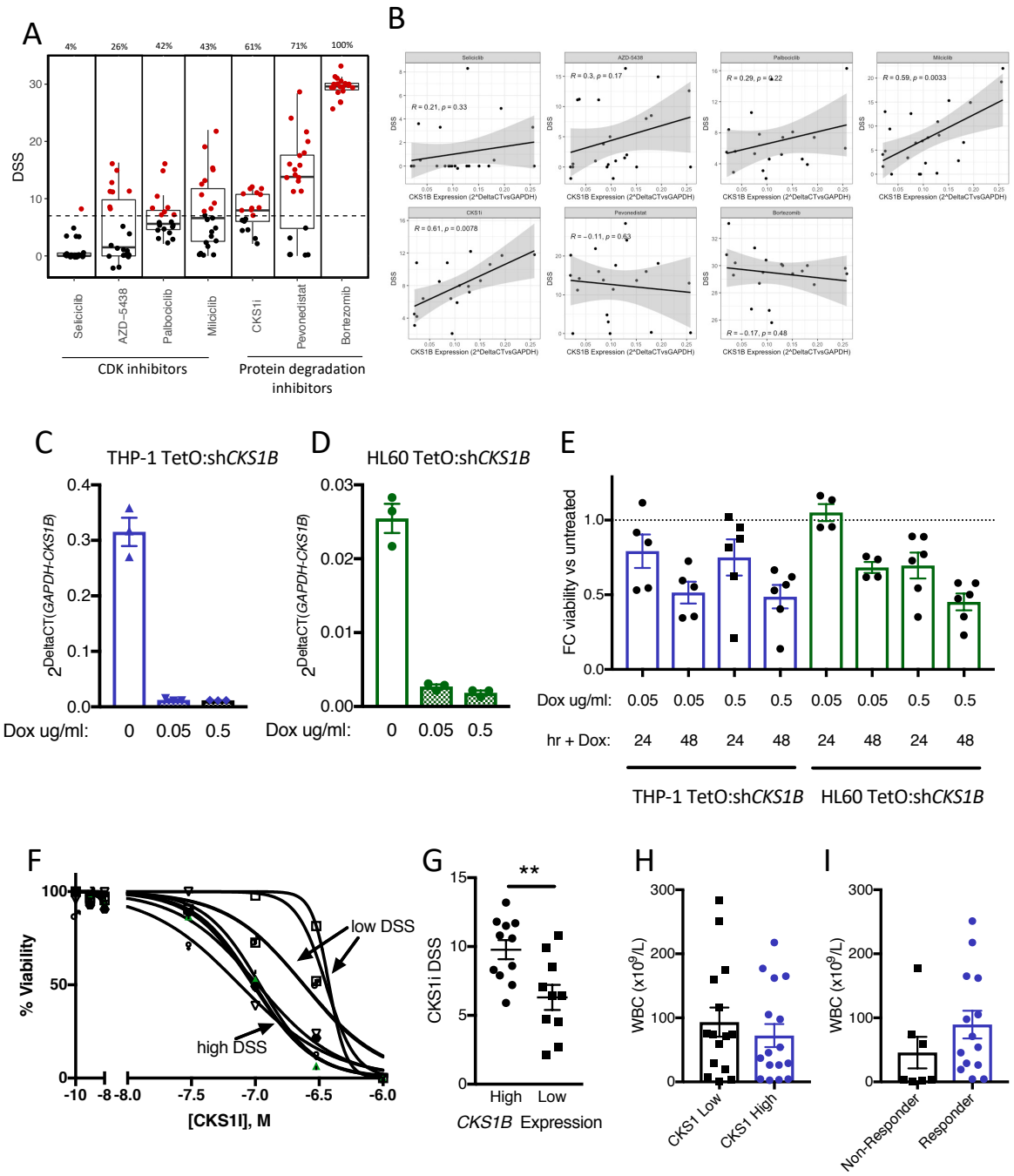

Supplementary Figure 2. Analysis of drug and genetic targeting of CKS1 in primary AML samples and AML cell lines A. Drug sensitivity score (DSS) for CDK

210 and protein degradation inhibitors in primary AML samples. Red indicates robust DSS
211 (>7), percentage above indicates proportion of patients with robust response. **B.**
212 Correlation between patient AML CKS1i drug sensitivity (DSS) and *CKS1B* expression
213 for the indicated drugs. 95% confidence intervals presented. Pearson's correlation
214 coefficient was calculated for correlation (R^2) and significance (*P*). Expression of
215 *CKS1B* in **C.** THP-1 and **D.** HL60 cells transduced with TetO:shRNA:*CKS1B* in
216 response to the indicated doses of doxycyclin after 24 hours. **E.** Fold change viability
217 compared to uninduced control THP-1 (Blue) and HL60 (Green) cells transduced with
218 TetO:shRNA:*CKS1B* in response to the indicated doses of doxycyclin for the indicated
219 time points. **F.** Example dose dependent response curves for primary patient AML
220 samples, indicating patient samples with high and low. **G.** CKS1i DSS grouped by
221 *CKS1B* expression cut at the 50th percentile. White blood cell counts ($x10^6$/L) of
222 patients with AML comparing **H.** *CKS1B* high versus low expression and **I.** CKS1i
223 responders versus non-responders. A Student's *t*-test was used to calculate
224 significance of difference for all graphs unless otherwise stated. ** $P<0.005$.

Supplementary Figure 3.

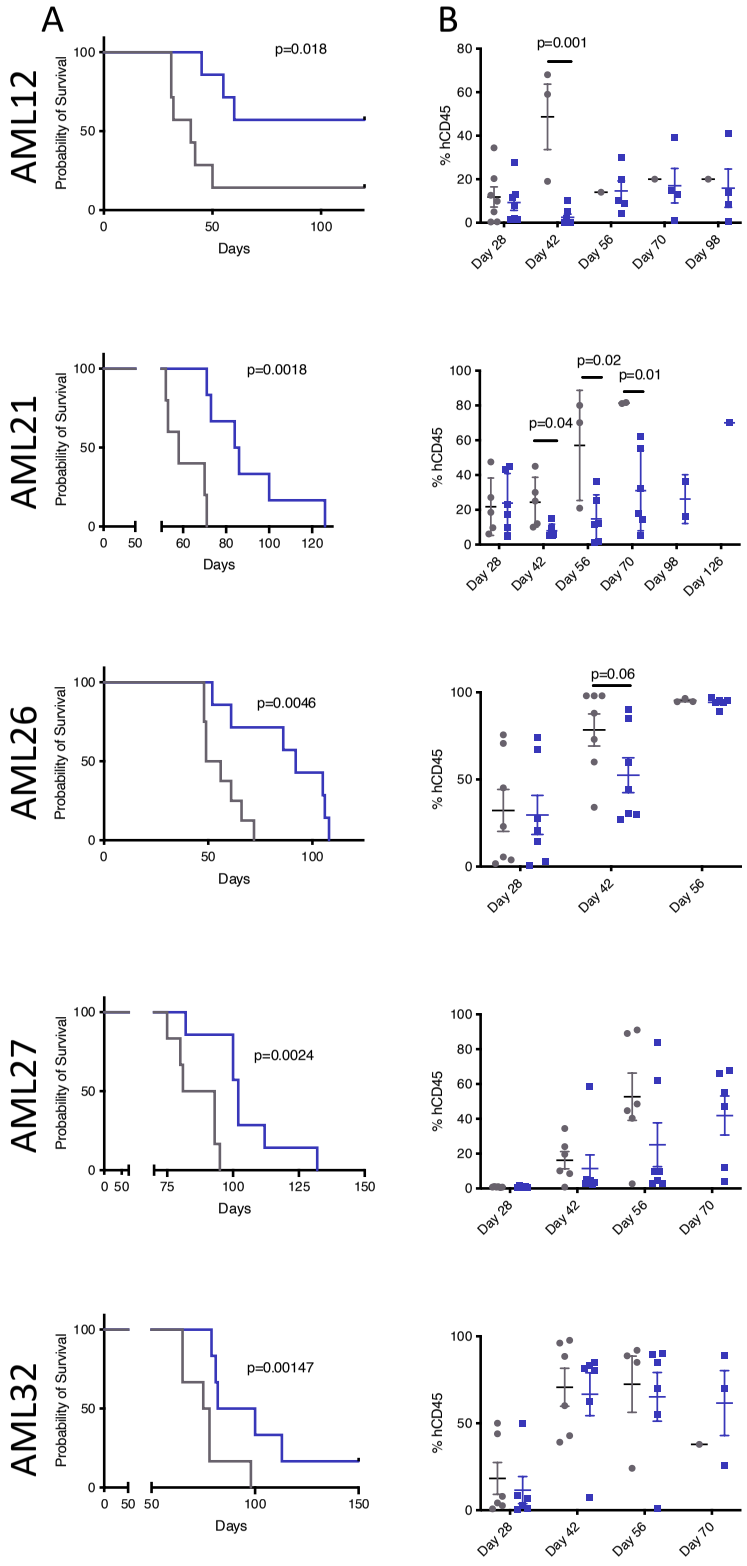

225

226

227 **Supplementary Figure 3. Overall survival and bone marrow engraftment of**
228 **patient derived xenografts. A.** Kaplan Meier plots representing overall survival and
229 **B.** Serial bone marrow aspirations for primary patient AML engrafted in NSG mice
230 (Control = Grey, CKS1i treated = Blue, AML12 Control *n* = 7 CKS1i *n* = 7, AML21
231 Control *n* = 5 CKS1i *n* = 6, AML26 Control *n* = 7 CKS1i *n* = 7, AML27 Control *n* = 6
232 CKS1i *n* = 7, AML32 Control *n* = 6 CKS1i *n* = 6).
233

234

Supplementary Figure 4.

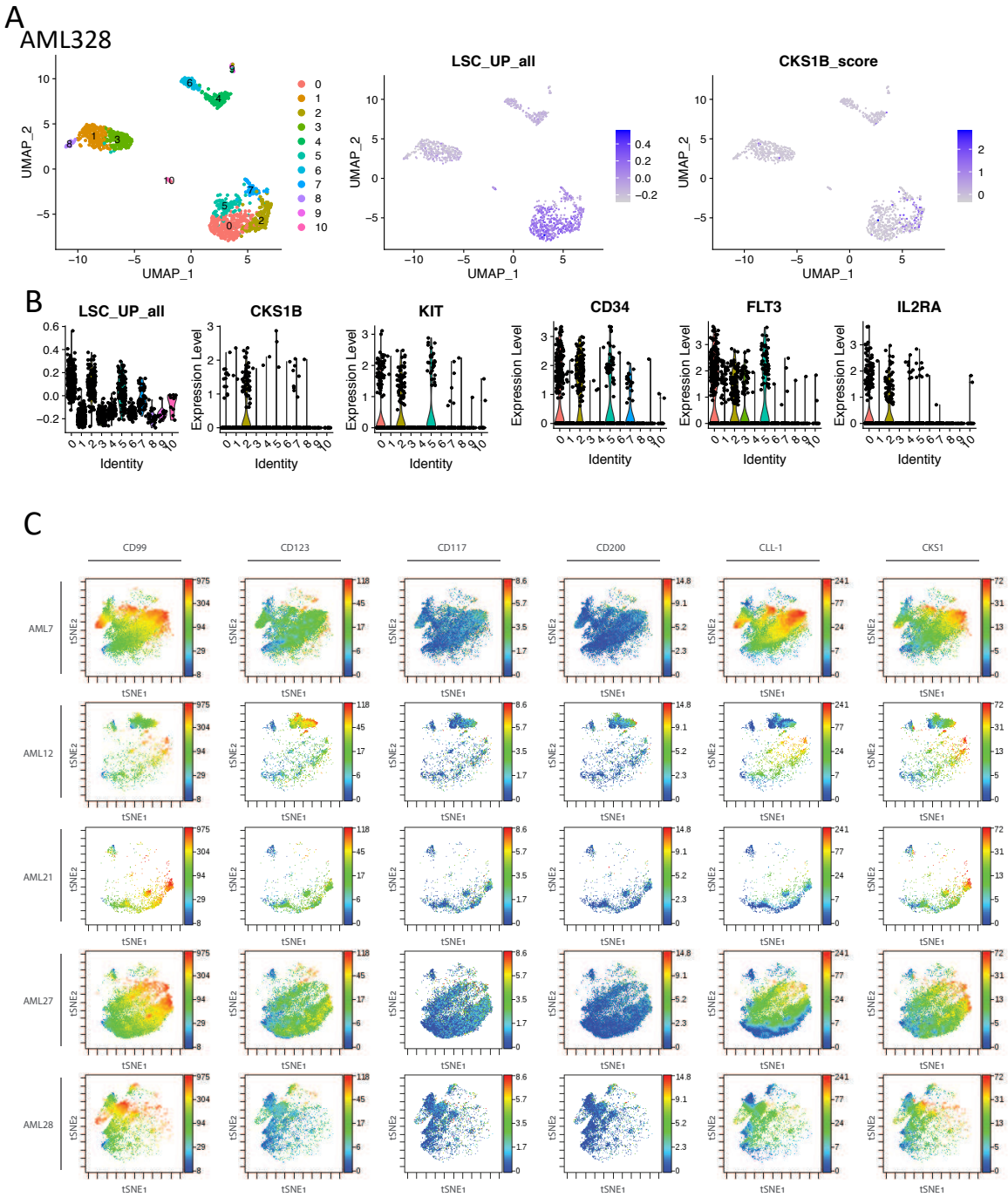

235

236 **Supplementary Figure 4. Analysis of CKS1 expression in AML LSCs. A-B.** Single
237 cell RNAseq analysis for patient AML328 obtained from van Galen *et al.* (2019).
238 Analyses present UMAP reductionality for cluster assignment, aggregated expression
239 of “LSC up” gene score from Ng *et al.* (2016), *CKS1B* expression and violin plots for
240 “LSC up” and individual genes. **C.** *t*-stochastic neighbour embedding of the indicated
241 patients from CyTOF analyses. All markers were used for dimensionality reduction,
242 key LSC cell surface markers and CKS1 are presented.
243
244
245

Supplementary Figure 5.

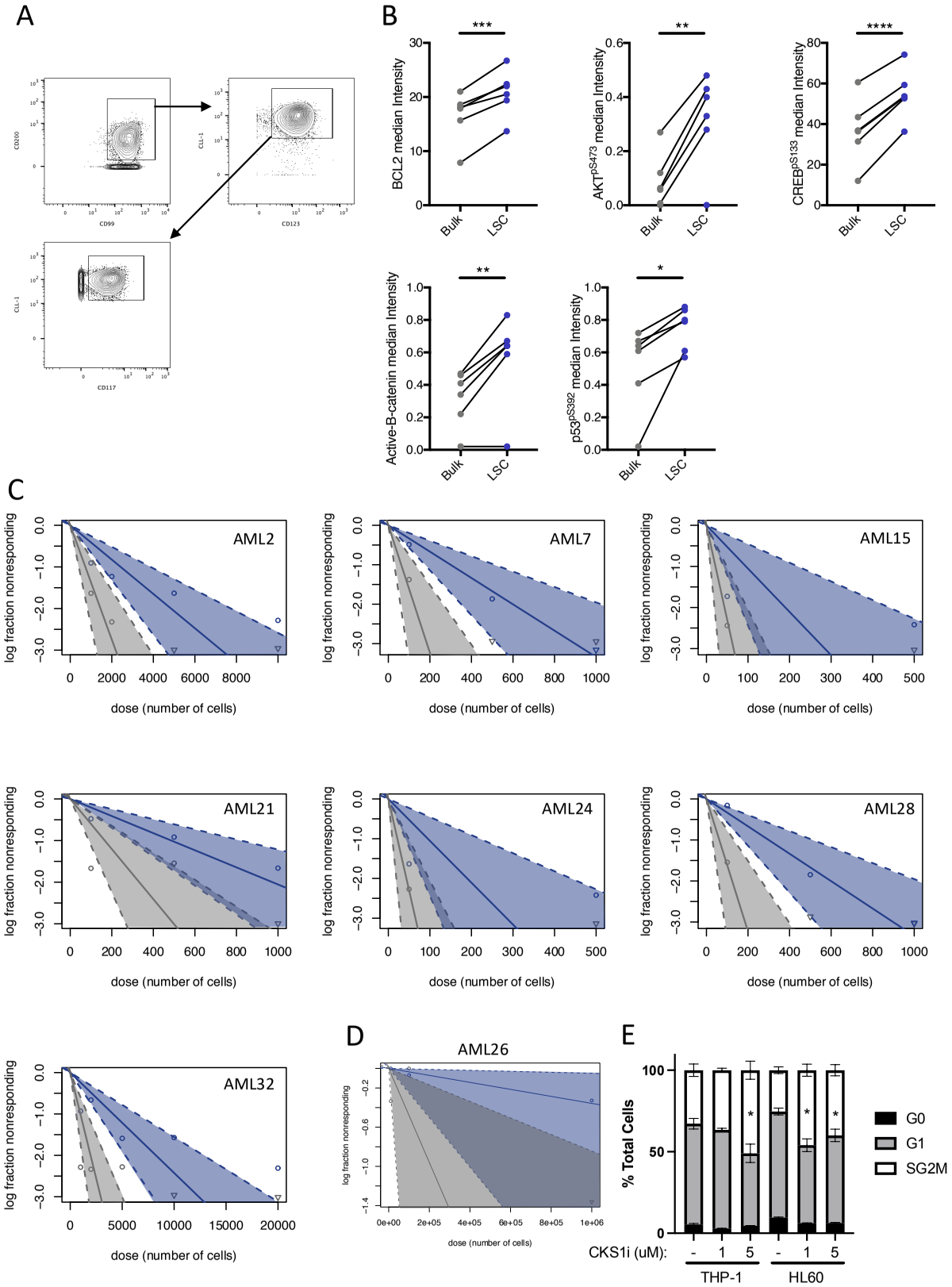

246

247

248 **Supplementary Figure 5. Patient AML LSC response to CKS1i. A.** Gating strategy
249 for defining LSCs in bulk AML samples. Cells were gated for live, single cells and de-
250 barcoded before example gating. **B.** Median intensity of the indicated proteins from
251 CyTOF analyses of Bulk AML and LSCs. **C.** Graph of estimated L-LTC-IC frequency
252 for the indicated patients control (grey) and treated with CKS1i (blue). **D.** Graph of
253 estimated LSC frequency for AML patient 26 treated in the primary xenograft with
254 control (grey) or CKS1i (blue). **E.** Cell cycle profiles of the indicated AML cell lines in
255 response to CKS1i after 24 hours.

Supplementary Figure 6

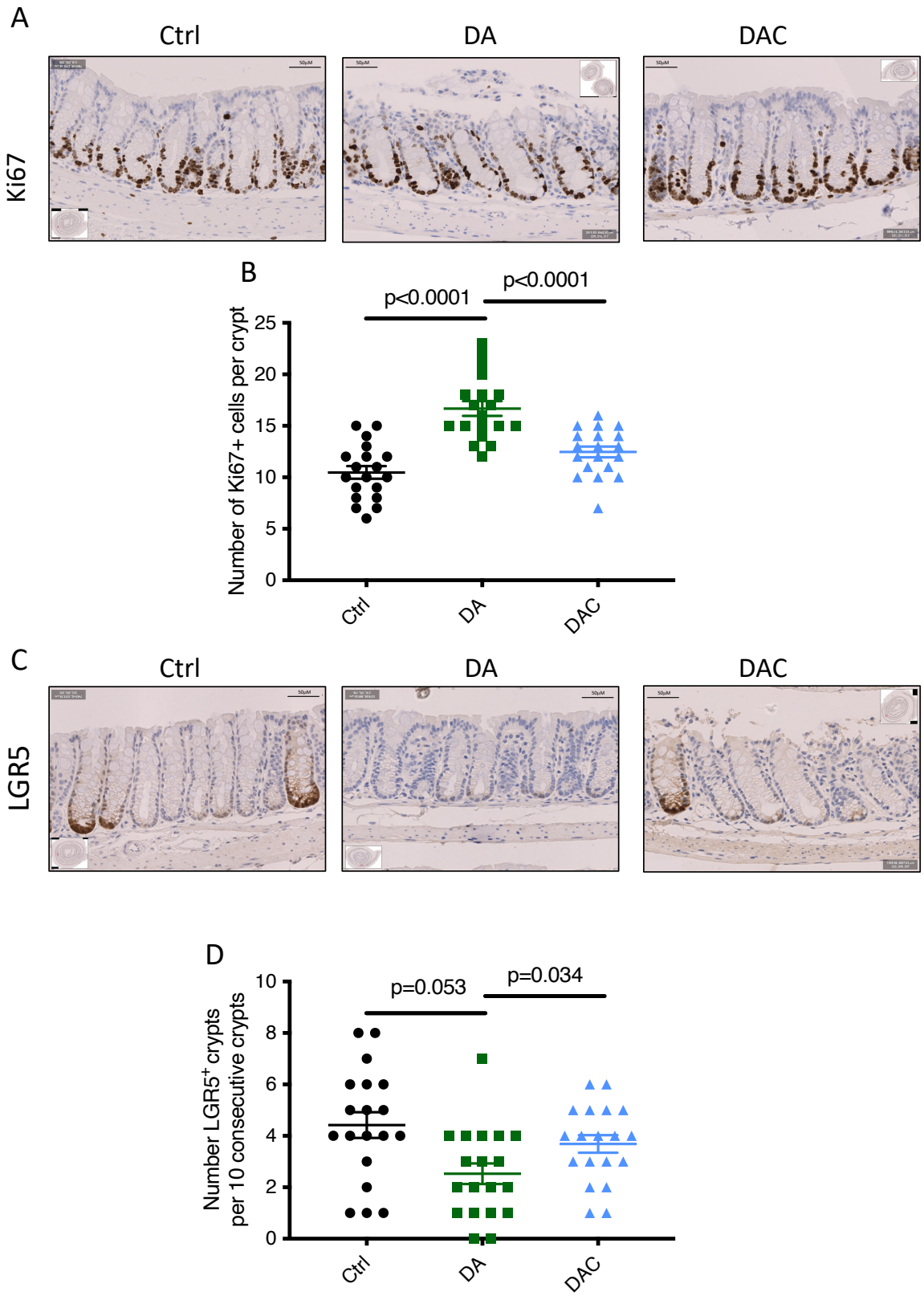

256

257

258 **Supplementary Figure 6 Effect of combination chemotherapy on mouse**
259 **intestinal crypts. A.** Representative intestinal crypts stained with Ki67 and **B.** Number
260 of Ki67 positive cells per crypt for the indicated treatments. **C.** Representative intestinal
261 crypts stained for anti-GFP in LGR5-GFP mice and **D.** Number of LGR5 positive crypts
262 per 10 consecutive crypts in intestinal preparations.
263

Supplementary Figure 7

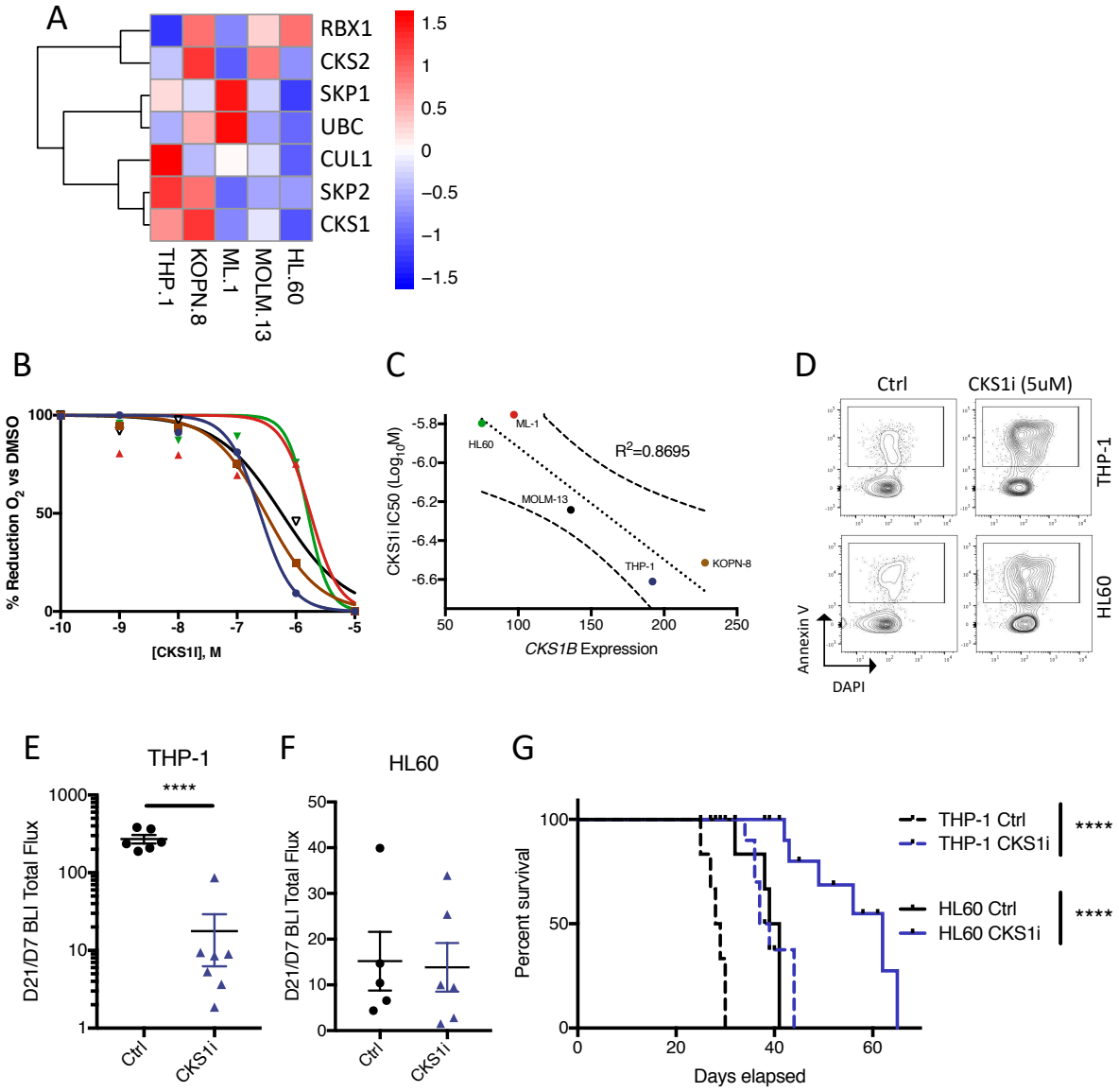

264

265

266 **Supplementary Figure 7. AML cell line *CKS1B* expression dictates CKS1i**
267 **sensitivity. A.** Expression of key $SCF^{SKP2\text{-}CKS1}$ subunits in leukemic cell lines used in
268 this study. Data presented are *z*-normalised (per gene) transcripts per million reads
269 (TPMs) from the EBI Cell Line Expression Atlas. **B.** Percentage viability of AML cell
270 lines cultured for 48 hours with indicated doses of CKS1i (*n*=3 for all cell lines on
271 graph). **C.** Correlation between AML cell line CKS1i IC_{50} and *CKS1B* expression. 95%
272 confidence intervals presented. Pearson's correlation coefficient was calculated for
273 correlation (R^2). **D.** Representative FACS plots for induction of apoptosis in the
274 indicated AML cell lines by presence of annexin V at the cell surface in response to
275 CKS1i (5μM) at 48 hours. Fold change in vivo leukemic burden of **E.** THP-1 (Ctrl *n*=6,
276 CKS1i *n*=7) and **F.** HL60 (Ctrl *n*=5, CKS1i *n*=6) cells day 21 (9 days post-CKS1i)
277 versus day 7 (pre-CKS1i) expressed as bioluminescent total flux intensity. **G.** Overall
278 survival of xenografts carrying THP-1 and HL60 cell lines control or treated with CKS1i.
279 A Student's *t*-test was used to calculate significance of difference for all graphs unless
280 otherwise stated. **** $P<0.00005$.
281

Supplementary Figure 8

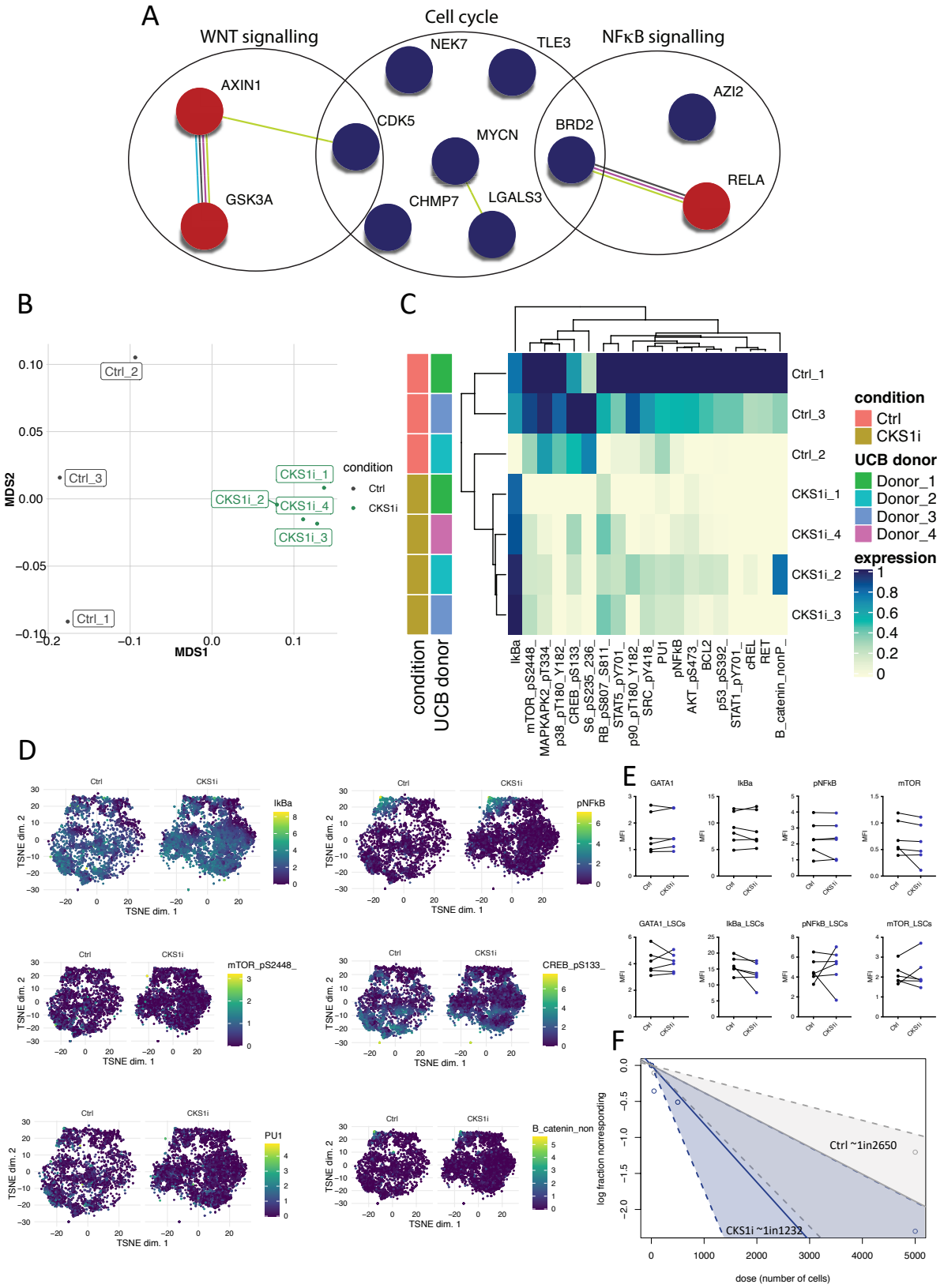

282

283

284 **Supplementary Figure 8. Effect of CKS1i on healthy hematopoiesis. A.** Key
285 proteins differentially abundant in $CD34^+$ cells in response to CKS1i (Red =
286 upregulated, Blue = downregulated). **B.** Pseudo-bulk-level multidimensional scaling
287 (MDS) plot for all markers used in mass cytometry analyses. **C.** Unsupervised
288 heatmap representing intracellular signalling markers in mass cytometric analyses *z*-
289 scaled for each marker. **D.** *t*-distributed stochastic neighbor embedding for control vs
290 CKS1i CyTOF samples with intensity scale for the indicated intracellular markers. **E.**
291 Intracellular signalling components measured in primary AML bulk (top panel) or LSCs
292 (bottom panel) post CKS1i treatment (1μM). **F.** LTC-IC estimated frequency of $CD34^+$
293 cells control (Grey) or treated with CKS1i (1μM, Blue).
294

Supplementary Figure 9

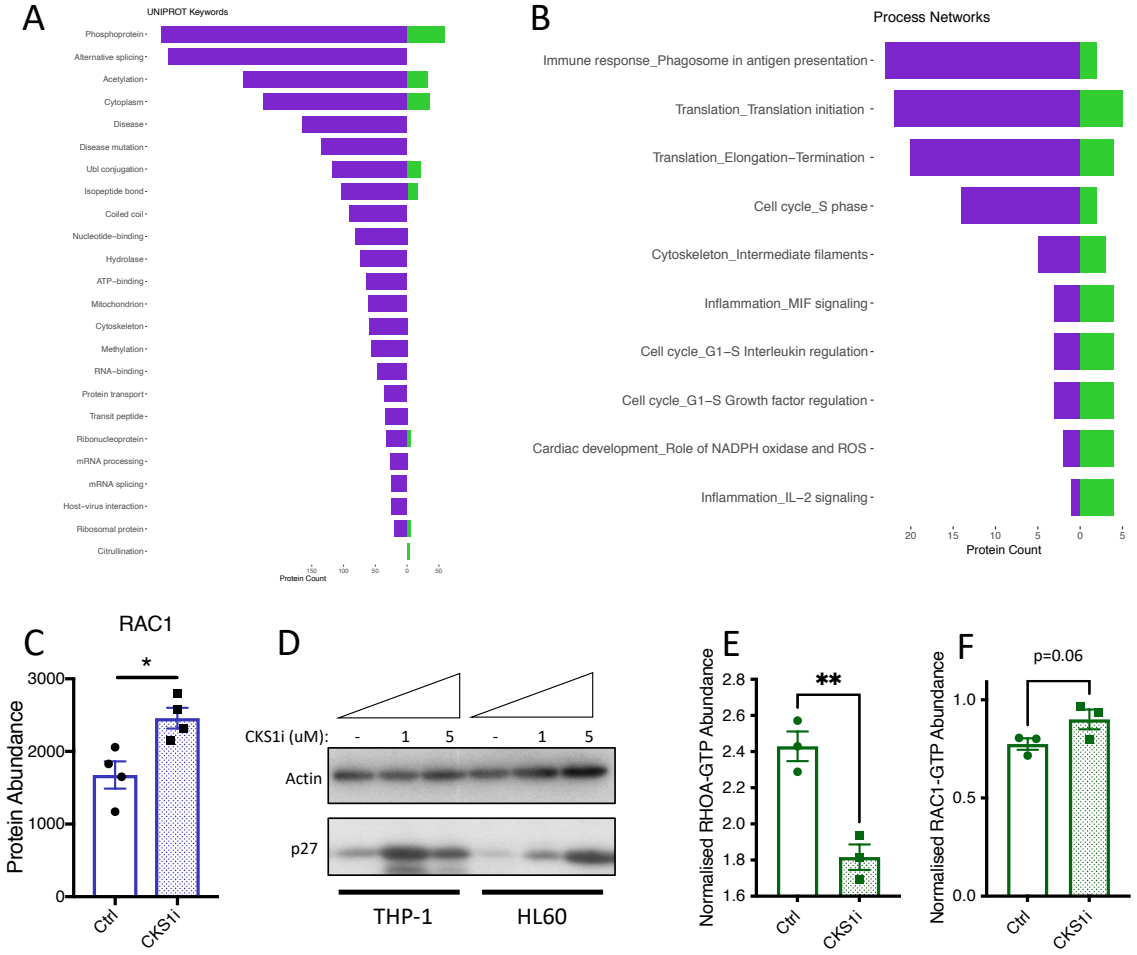

295

296

297

298 **Supplementary Figure 9. Effect of CKS1i on AML cell lines. A.** Uniprot keywords
299 and **B.** Process networks from differentially abundant proteins in THP-1 (purple) and
300 $CD34^+$ (green) cells. **C.** Abundance of RAC1 protein in THP-1 cells treated with CKS1i
301 (1μM) from mass spectrometry analyses. **D.** Western blot for p27 in AML cell lines in
302 response to the indicated doses of CKS1i after 24 hours. **E.** RHOA-GTP and **F.** RAC1-
303 GTP abundance in HL60 cells treated with CKS1i (1μM). A Student's t-test was used
304 to calculate significance of differences. * $P<0.05$, ** $P<0.005$.
305

Supplementary Figure 10

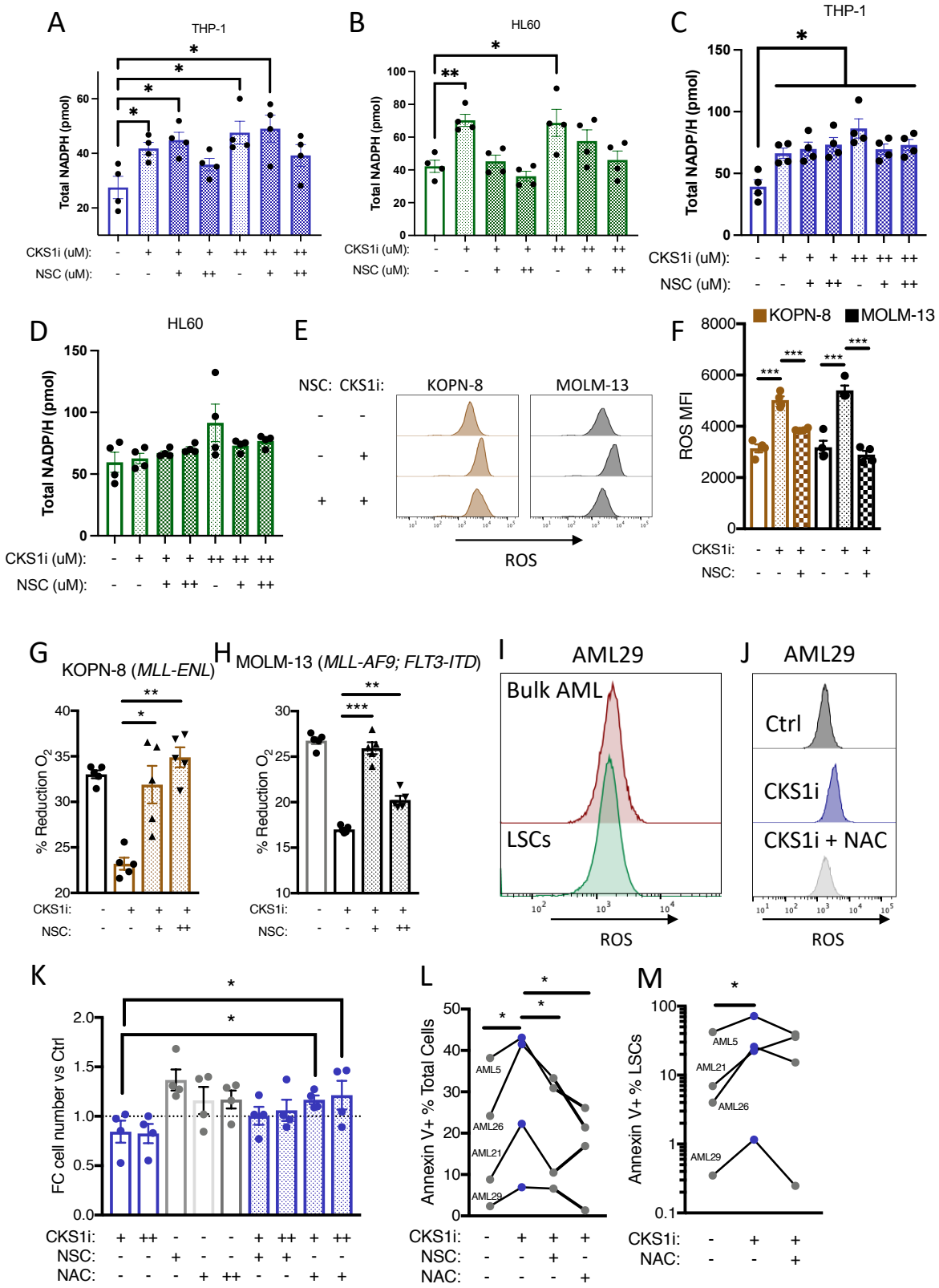

306

307

308 **Supplementary Figure 10. CKS1i induces NADPH accumulation and lethal ROS**
309 **in AML.** Total NADPH (pmol) in **A.** THP-1 and **B.** HL60 cells treated for 8 hours with
310 the indicated doses of CKS1i (+ = 1μM, ++ = 5μM) and NSC (+ = 0.1μM, ++ = 1μM).
311 Total NADP/NADPH (pmol) in **C.** THP-1 and **D.** HL60 cells treated for 8 hours with the
312 indicated doses of CKS1i (+ = 1μM, ++ = 5μM) and NSC (+ = 0.1μM, ++ = 1μM). **E.**
313 Representative flow plots and **F.** Quantified mean fluorescence intensity of
314 intracellular reactive oxygen species (ROS) in the indicated cell lines in response to
315 CKS1i (+ = 1μM) and NSC (+ = 0.1μM) treatment (N=3 per cell line and treatment).
316 Viability represented by percentage reduction O_2 of **G.** KOPN-8 and **H.** MOLM-13 cells
317 in response to the indicated concentrations of CKS1i and NSC (N=5 per cell line and
318 treatment, except THP-1 where N=6), CKS1i (+ = 1μM) and NSC (+ = 0.1μM, ++ =
319 1μM). **I.** Intracellular ROS measured in primary patient AML bulk vs LSC fraction. **J.**
320 Intracellular ROS measured in primary AML cultured in control conditions, with CKS1i
321 (1μM) or CKS1i + NAC (1μM + 1.25mM). **K.** Fold change absolute live cell number of
322 patient AMLs compared to controls for the indicated treatments (CKS1i + = 1μM, ++ =
323 5μM, NSC + = 0.1μM, NAC + = 1.25mM, ++ = 2.5mM). Each point represents one
324 primary patient AML sample. Percentage of annexin V positive cells of **L.** total primary
325 patient AMLs and **M.** immunophenotypic LSCs with the indicated treatments (CKS1i +
326 = 1μM, ++ = 5μM, NSC + = 0.1μM, NAC + = 1.25mM, ++ = 2.5mM). A Student's *t*-test
327 was used to calculate significance of difference for all graphs * $P<0.05$; ** $P<0.05$;
328 *** $P<0.005$.
329

Supplementary Figure 11

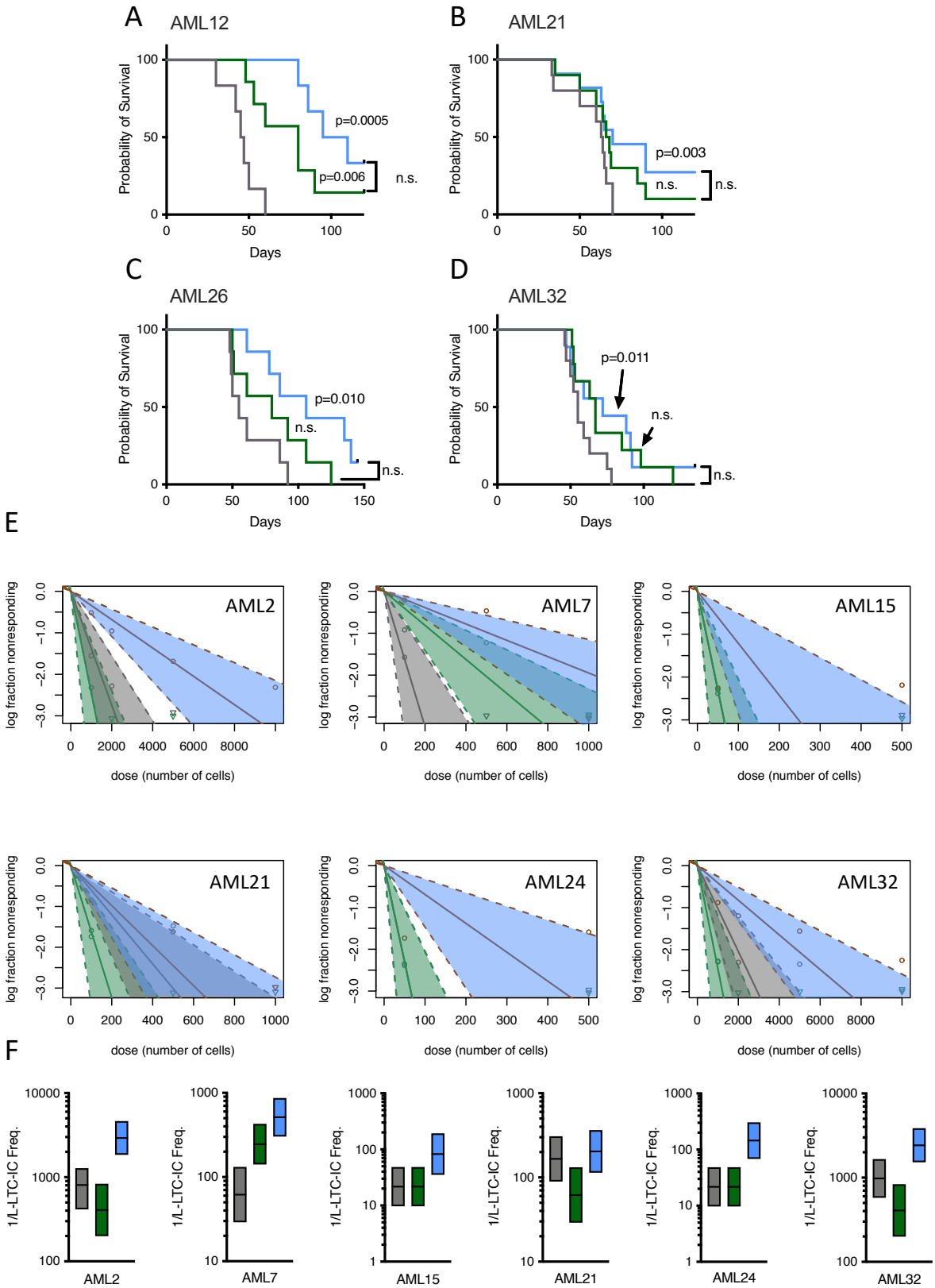

332 **Supplementary Figure 11. In vivo and ex vivo response of patient AML samples**
333 **to CKS1i. A-D.** Kaplan Meier graphs for the indicated patient AML xenograft cohorts
334 (Grey = control, green = DA, blue = DAC, AML12 control *n* = 6 DA *n* = 7 DAC *n* = 7,
335 AML21 control *n* = 10 DA *n* = 10 DAC *n* = 11, AML26 control *n* = 7 DA *n* = 7 DAC *n* =
336 7, AML32 control *n* = 10 DA *n* = 9 DAC *n* = 9). **E.** Graph of estimated L-LTC-IC
337 frequency for the indicated patients' control (Grey) and treated with DA (Green) or
338 DAC (Blue). **F.** Calculated L-LTC-IC frequencies and confidence intervals by ELDA
339 (Control = Grey, DA = Green, DAC = Blue).
340

Supplementary Figure 12

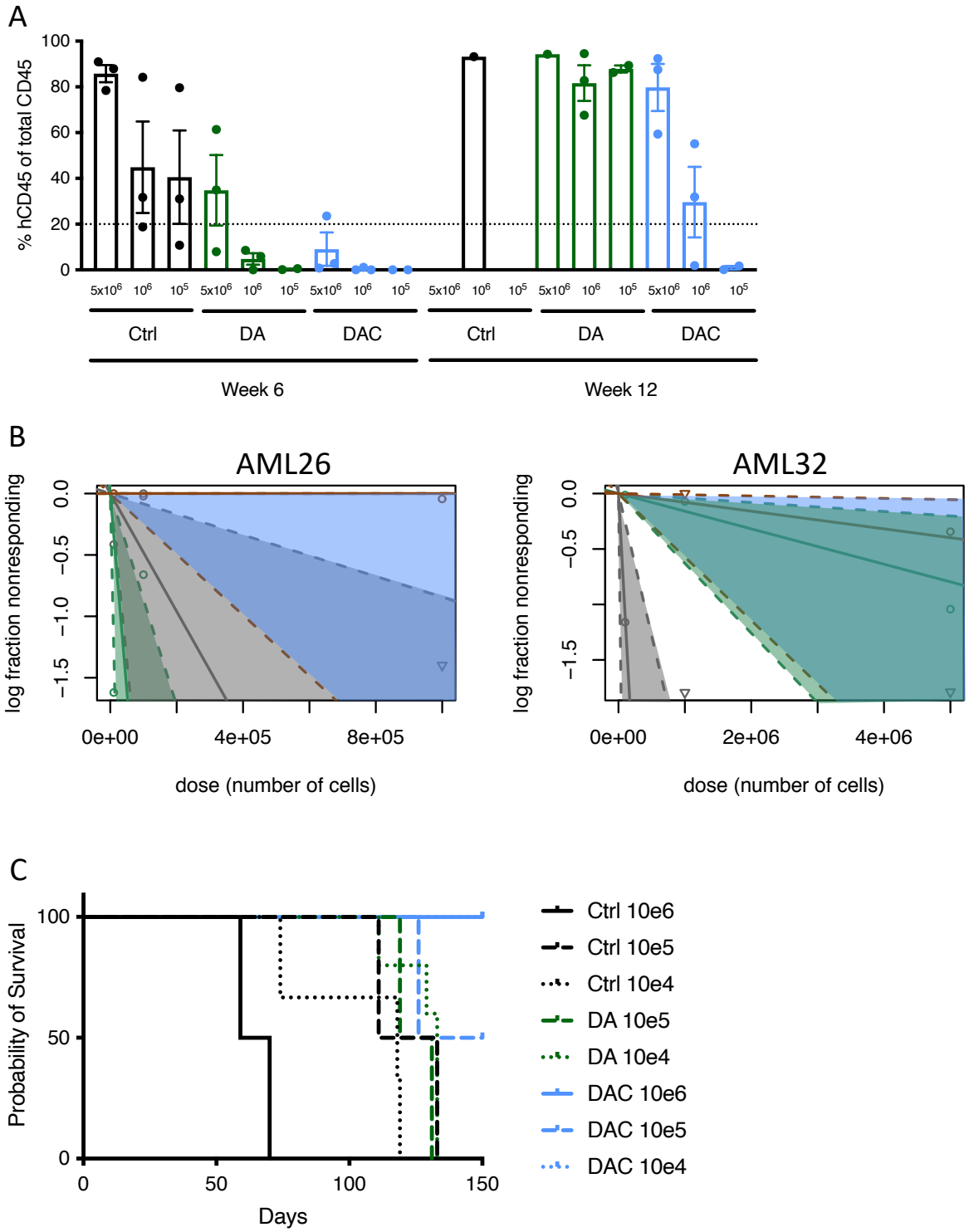

343 **Supplementary Figure 12. Secondary transplantation of patient AML samples**
344 **previously treated with chemotherapy. A.** Percentage hCD45 bone marrow
345 engraftment of AML32 engrafted in secondary mice at limiting dilution weeks 6 and 12
346 (Ctrl n = 3 per dose, DA $5x10^6$ & 10^6 n = 3 per dose; 10^5 n = 2, DAC $5x10^6$ & 10^6 &
347 10^5 n = 3 per dose). **B.** Graph of estimated LSC frequency for the indicated patients'
348 control (Grey) and treated with DA (Green) or DAC (Blue). **C.** Overall survival of
349 secondary transplantation mice from primary AML32 PDX control (Black) or treated
350 with DA (Green) or DAC (Blue).
351

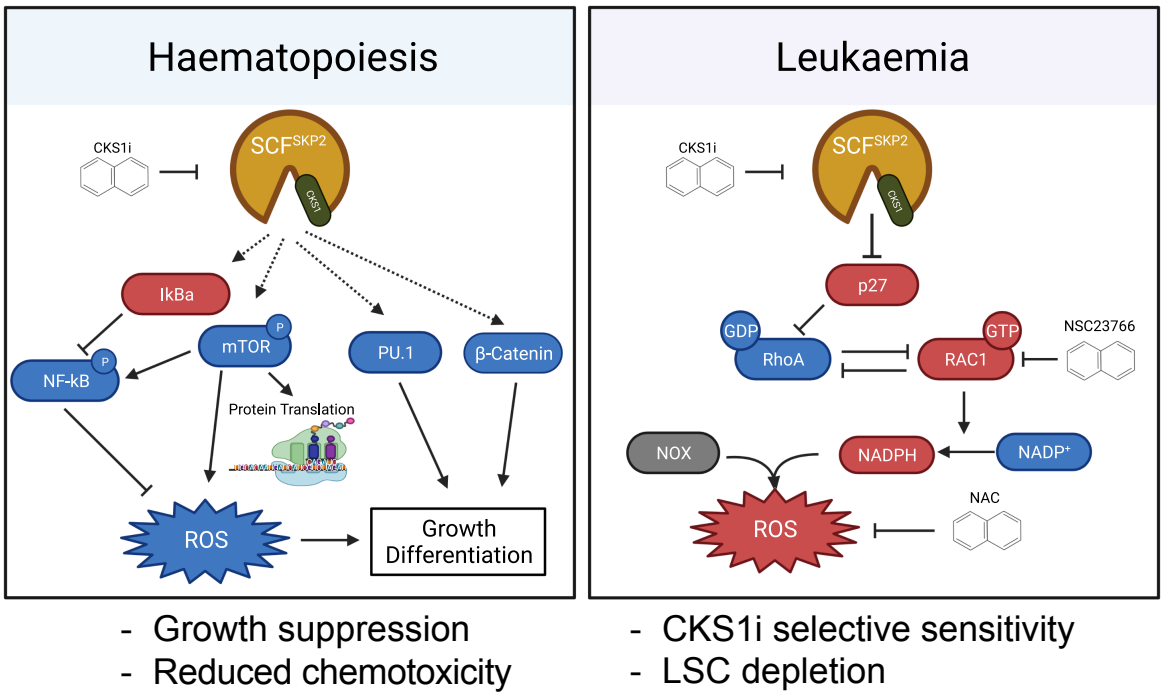

- Growth suppression
- Reduced chemotoxicity

- CKS1i selective sensitivity
- LSC depletion

Graphical abstract. Model for mechanism of action for CKS1i in healthy hematopoiesis and leukemia.